

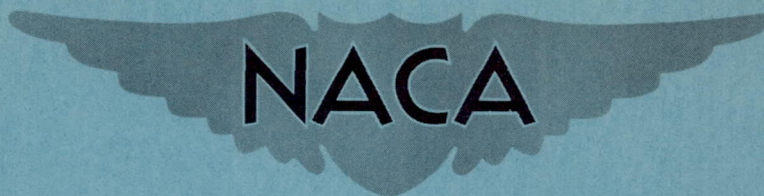
FILE COPY  
NO 6

CONFIDENTIAL

Copy 158

RM A9G15

NACA RM A9G15



# RESEARCH MEMORANDUM

THE EFFECT OF THE PROPELLER SLIPSTREAM ON THE  
CHARACTERISTICS OF SUBMERGED INLETS

By Noel K. Delany

Ames Aeronautical Laboratory

THIS DOCUMENT ON LOAN FROM THE FILES OF Moffett Field, Calif.

NATIONAL ADVISORY COMMITTEE FOR AERONAUTICS  
LANGLEY AERONAUTICAL LABORATORY  
LANGLEY FIELD, HAMPTON, VIRGINIA

CLASSIFICATION CHANGED TO

UNCLASSIFIED

DATE 8-18-54

AUTHORITY J.W.CROWLEY

RETURN TO THE ABOVE ADDRESS.

REQUESTS FOR PUBLICATIONS SHOULD BE ADDRESSED  
AS FOLLOWS:

CHANGE # 2448

W.H.L.

NATIONAL ADVISORY COMMITTEE FOR AERONAUTICS  
1512 H STREET, N. W.  
WASHINGTON 25, D. C.

CLASSIFIED DOCUMENT

This document contains classified information affecting the National Defense of the United States within the meaning of the Espionage Act, USC 50:31 and 32. Its transmission or the revelation of its contents in any manner to an unauthorized person is prohibited by law. Information so classified may be imparted only to persons in the military and naval services of the United States, appropriate civilian officers and employees of the Federal Government who have a legitimate interest therein, and to United States citizens of known loyalty and discretion who of necessity must be informed thereof.

NATIONAL ADVISORY COMMITTEE  
FOR AERONAUTICS

WASHINGTON  
September 9, 1949

CONFIDENTIAL







## NATIONAL ADVISORY COMMITTEE FOR AERONAUTICS

RESEARCH MEMORANDUMTHE EFFECT OF THE PROPELLER SLIPSTREAM ON THE  
CHARACTERISTICS OF SUBMERGED INLETS

By Noel K. Delany

## SUMMARY

A wind-tunnel investigation has been made to determine the effect of propeller operation on the characteristics of submerged inlets. The tests were performed with a model of a hypothetical fighter airplane powered by a turbine-propeller unit. The propeller had eight blades with thin airfoil shanks and had dual rotation. The submerged inlets were placed in the fuselage behind the propeller and forward of the wing.

It was found that for zero thrust there was a loss of ram-pressure recovery due to the propeller that varied with blade angle and with angle of attack. However, as the thrust coefficient was increased the ram-pressure recovery increased and eventually exceeded that obtained with the propeller removed. The rate of increase of the ram-pressure recovery with propeller thrust coefficient was relatively independent of inlet-velocity ratio, but decreased with increasing propeller-blade angle and with angle of attack. In general, it was found that the effect of propeller operation on the ram-recovery ratio was the same with either parallel- or divergent-walled entries.

## INTRODUCTION

Previous investigations of models without propellers have shown that NACA submerged air inlets (references 1 and 2) will operate efficiently when properly located in the sides of fuselages. For an application of submerged air inlets on a propeller-driven aircraft, the effects of the propeller on the characteristics of the inlet should be considered. To maintain a high ram-pressure recovery for the inlet, the propeller should not cause pressure losses and, if possible, should increase the pressure ahead of the inlets. Thick propeller shanks would probably cause excessive pressure losses, particularly for the relatively low values of propeller thrust coefficient encountered in high-speed flight where high ram recovery assumes great importance. Also, for forward speeds at which the force-divergence Mach number



of the shank sections is exceeded, the pressure losses at the inlets would be increased over those for lower speeds. Propellers with thin shank sections and proper blade angles near the spinner should provide the best ram-pressure-recovery characteristics.

An experimental investigation was undertaken to evaluate the effects of a propeller with relatively thin shanks on the ram-pressure recovery of submerged inlets at low Mach numbers. The model used for the research reported in reference 1 was utilized for the study and was provided with an eight-blade dual-rotation propeller. The ram-pressure recovery was measured for a wide range of angle of attack, blade angle, propeller thrust coefficient, advance-diameter ratio, and inlet-velocity ratio, which bracketed typical values of these variables for fighter-type airplanes.

The test results were obtained in the Ames 7- by 10-foot wind tunnel No. 2 at the request of the Bureau of Aeronautics, Navy Department.

#### SYMBOLS

The following symbols have been used in the presentation of the test results:

A	duct cross-sectional area, square feet
b	chord of a propeller-blade element, feet
D	propeller diameter, feet
H	total pressure, pounds per square foot
h	maximum thickness of a propeller-blade element, feet
J	advance-diameter ratio $\left(\frac{V}{nD}\right)$
n	propeller rotational speed, revolutions per second
P	geometric pitch of a propeller-blade element ( $2\pi r \tan \beta'$ ), feet
p	static pressure, pounds per square foot
q	dynamic pressure, pounds per square foot
R	propeller-tip radius, feet
r	radius to a propeller-blade element, feet



S	wing area, square feet
V	true air velocity, feet per second
V'	true air velocity, miles per hour
$\alpha_u$	uncorrected angle of attack, measured with respect to the fuselage reference line, degrees
$\beta'$	blade angle of an element, degrees
$\beta$	blade angle at $r/R = 0.75$ , degrees
$\delta$	ratio of atmospheric pressure at altitude to standard atmospheric pressure at sea level
$\theta$	ratio of absolute atmospheric temperature at altitude to standard absolute atmospheric temperature at sea level
$\rho$	mass density of air, slugs per cubic foot
$\sigma$	ratio of the mass density of the air at altitude to the standard mass density of the air at sea level
$C_L$	lift coefficient $\left(\frac{\text{lift}}{q_0 S}\right)$
$C_p$	propeller power coefficient $\left(\frac{\text{input power}}{\rho_0 n^3 D^5}\right)$
$\frac{H-p_0}{H_0-p_0}$	ram-recovery ratio
$T_c$	propeller thrust coefficient $\left(\frac{\text{net thrust}}{\rho_0 V_0^2 D^2}\right)$
$\frac{V_1}{V_0}$	inlet-velocity ratio
$\frac{W}{S}$	wing loading $\left(\frac{\text{airplane gross weight}}{S}\right)$ , pounds per square foot

Subscripts used to define further the above are as follows:

- 0 free-stream
- 1 duct entrance (1.50 in. behind lip leading edge)
- 2 inlet to the compressor



## DESCRIPTION OF THE MODEL

The 1/4-scale model used in this investigation was that described in reference 1, with the addition of a dual-rotating tractor propeller. The pertinent model dimensions and a three-view drawing of the hypothetical airplane it represents are presented in the appendix and in figure 1, respectively. A photograph of the model without the propeller is shown in figure 2.

Two types of submerged inlets were tested: One had a ramp with parallel walls, and the other a ramp with diverging walls (fig. 3). The lips of the model inlets were 20.66 inches behind the plane of the rear propeller blades and the center lines of the ramps were 1.05 inches below the thrust axis. The detailed dimensions and coordinates of the submerged inlets are presented in reference 1. The internal ducting corresponded to the short internal ducting utilized in the research reported in reference 1.

The propeller, shown in figure 4, was 3 feet in diameter and the blades had NACA 16-series sections with broad, thin shanks. Approximate values of the blade thickness at the spinner were 0.14 chord for the front propeller blades and 0.12 chord for the rear propeller blades. The propeller used had NACA 3-(3.9)(07)-0345-A blades and the blade-form curves are shown in figure 5. The spinner diameters were 20.2 and 26.0 percent of the propeller diameter in the planes of the front and rear propeller blades, respectively. The blades passed through openings in the spinner which were only large enough to allow the blade angle to be changed from  $35^{\circ}$  to  $55^{\circ}$ . The gaps between the blade shanks and the spinner were not sealed. A 110-horsepower variable-speed electric motor was used to drive the model propeller.

## TEST METHODS AND REDUCTION OF DATA

The quantity of air flowing into the submerged air inlets of the model was controlled by a centrifugal pump outside of the wind tunnel. The ram-pressure recovery at the duct inlets and at the simulated entrance to the compressor and the velocity ratio at the inlet were computed in the manner described in reference 1.

The net thrust of the model propeller was calculated as the difference between the force in the drag direction with the propeller operating and the force with the propeller removed. The input power to the propeller was computed from the motor input power and the motor efficiency. Figure 6 shows the characteristics of the propeller on the model.

Preliminary tests were made with and without the gaps between the propeller and the spinner sealed, and the effect on the ram-pressure recovery was not noticeable. Consequently, because of mechanical



difficulties, the data were obtained with the gaps between the blade shanks and the spinner open. It was mentioned in reference 3, however, that the gaps between the surface of the spinner and the blade shanks may reduce the propeller efficiency several percent.

Figure 7 shows the variation of the shaft horsepower with flight speed for the turbine-propeller unit assumed to be used in the hypothetical airplane. The full-scale-operation parameters of the propeller (fig. 8) were estimated for a propeller rotating at 1200 rpm, using the turbine shaft horsepower of figure 7 and the propeller data of figure 6. Figure 9 shows the estimated variation of the inlet-velocity ratio with flight speed. The variations of the lift coefficient and the flight speed with angle of attack are shown in figure 10.

## RESULTS AND DISCUSSION

### Limitations of Data

Differences between the characteristics of the model propeller used in this investigation and the propeller for an airplane installation, particularly the thrust loading near the blade shanks, would probably cause differences in inlet characteristics with the propeller operating. Since the results were obtained at low Mach numbers (0.13 to 0.19), the test conditions simulating flight at high speeds were not truly representative of conditions at high speeds. Reference 3 shows that for the propeller used in these tests the thin shank sections were more highly loaded at high subsonic Mach numbers than at low subsonic Mach numbers. This change in the thrust distribution with Mach number may result in an increase of the available ram pressure in the slipstream where the inlets are located as long as the force-divergence Mach number of the shank sections is not exceeded. The results of tests of an airplane model without a propeller and with NACA submerged inlets ahead of the wing (reference 2) indicated that the ram-pressure recovery was not severely affected by compressibility to a Mach number of 0.875. However, when the inlets were behind the wing leading edge, the ram-pressure recovery decreased at Mach numbers as low as 0.70 (reference 4).

### Distribution of Ram Pressure in Slipstream

Without the submerged inlets in the model, surveys of the total pressure over the forward portion of the fuselage were made with the propeller operating and with the propeller removed. Figures 11 and 12 present the increments expressed in terms of ram-recovery ratio obtained from these surveys for blade angles of  $35^\circ$  and  $55^\circ$ . Close to the fuselage surface a decrease in the increment of ram pressure due to the propeller was evident for low thrust coefficients. For a blade angle of  $35^\circ$  and a thrust coefficient of zero, the loss in ram pressure, averaged



over a height equal to the depth of the inlet at the lip, was 15 percent of the free-stream ram pressure. This loss of ram pressure was caused by the shank sections of the propeller blades which were producing negative thrust. The losses due to the shanks were not as great at a blade angle of  $55^\circ$ . An attempt was made to compute the change in the ram pressure due to the propeller by strip theory, but satisfactory results were not obtained in the region of interest near the shanks.

#### Effect of the Propeller on Ram-Recovery Ratio

The effect on the ram-recovery ratio of varying the propeller thrust coefficient is shown in figures 13 to 22 for several inlet-velocity ratios, angles of attack, and blade angles. The ram-pressure recovery was measured both at the inlet and at the simulated entrance to the compressor. These measurements were made for inlets having parallel ramp walls and for inlets having diverging ramp walls at angles of attack of  $-2^\circ$  to  $6^\circ$ . The following table shows the extent of the variables investigated and the figures in which the results are presented:

Type of inlet	Survey station	$V_1/V_0$	$T_c$	$\beta$ (deg)	Figure
Parallel ramp walls	Duct entrance	0.6 to 1.6	0 to 0.15	35	13
Do.	Do.	.5 to 1.0	0 to .05	55	14
Diverging ramp walls	Do.	.6 to 1.6	0 to .15	35	15
Do.	Do.	.5 to 1.0	0 to .05	55	16
Parallel ramp walls	Compressor entrance	.8 to 1.6	0 to .15	35	17
Do.	Do.	.5 to 1.0	0 to .10	45	18
Do.	Do.	.5 to 1.0	0 to .05	55	19
Diverging ramp walls	Do.	.5 to 1.6	0 to .15	35	20
Do.	Do.	.5 to 1.0	0 to .10	45	21
Do.	Do.	.5 to 1.0	0 to .03	55	22

Effect of thrust coefficient.— The data in figures 13 to 22, inclusive, show that for all of the conditions investigated the ram-pressure recovery increased as the thrust coefficient was increased. The rate of change of the ram-recovery ratio with thrust coefficient

$\frac{d(H-p_0)/(H_0-p_0)}{dT_c}$  was relatively independent of inlet-velocity ratio



and approximately the same at the entrance of the inlet or at the simulated entrance of the compressor for both parallel- and divergent-walled ramps. Figure 23 shows the variation of the average values of  $\frac{d(H-p_o)/(H_o-p_o)}{dT_c}$ , obtained from figures 13 to 22, with angle of attack and with propeller-blade angle. For constant propeller-blade angles  $\frac{d(H-p_o)/(H_o-p_o)}{dT_c}$  decreased linearly as the angle of attack was increased.

A comparison of the variation with thrust coefficient of the ram pressure added by the propeller (fig. 12), averaged over a distance from the fuselage equal to the depth of the inlet, with the data of figure 23 shows good agreement. By the use of the incompressible momentum theory

for propellers, a value of  $\frac{d(H-p_o)/(H_o-p_o)}{dT_c} = \frac{8}{\pi}$  would be predicted for

the average of the entire propeller slipstream. This theory, however, does not take into account the effects of changes in the radial distribution of the propeller thrust.

Effect of angle of attack.— The data in reference 1 show that the ram-pressure recovery for the model without the propeller decreased slightly with increasing angle of attack. However, with the propeller installed and operating at zero thrust coefficient (figs. 13 to 22), the ram-recovery ratio increased approximately 0.01 per degree increase of angle of attack in the range of the tests. A possible explanation for the increase of the ram-recovery ratio with angle of attack may be that the slipstream tended to follow the free-stream direction rather than the thrust axis, thus placing the submerged inlets in a region of the slipstream that had a higher ram pressure.

Effect of blade angle.— As previously mentioned in the discussion of the total pressures behind the propeller, increasing the blade angle at constant thrust coefficient increased the ram pressure near the fuselage immediately behind the propeller. Increasing the blade angle had a similar effect on the ram-recovery ratio at the inlets and at the entrance to the compressor, as shown in figures 24 and 25. The data obtained with the propeller removed (reference 1) are also shown in figures 24 and 25. The decrement of ram-pressure recovery due to the propeller operating with zero thrust is given in the following table for an inlet-velocity ratio of 0.7 and an angle of attack of 0°:

$\beta$ (deg)	Duct entrance		Compressor entrance	
	Parallel ramp walls	Diverging ramp walls	Parallel ramp walls	Diverging ramp walls
35	0.18	0.18	0.14	0.15
45	—	—	.12	.12
55	.09	.09	.09	.10



### Simulated Flight Conditions

The ram-pressure recoveries are presented in figures 26 and 27 for conditions simulating the lift coefficient, inlet-velocity ratio, propeller thrust coefficient, blade angle, and advance-diameter ratio (derived from figs. 8 to 10 and 13 to 22) for the hypothetical airplane. The data for the same model without a propeller (reference 1) are also presented to show the over-all effects of the propeller operating with full engine power. The effect of the propeller operation was approximately the same whether measured at the inlet or at the entrance to the compressor for both parallel- and divergent-walled inlets. The ram-recovery ratio was reduced approximately 0.06 by the propeller for conditions simulating flight at 500 miles per hour. For a climb condition (250 mph) the propeller increased the ram-pressure recovery. The change in the ram-pressure recovery with increased altitude for a constant velocity is the result of the increased inlet-velocity ratio and increased angle of attack, and of the decreased propeller-blade angle and thrust coefficient necessary at the higher altitude.

### CONCLUSIONS

The following conclusions are drawn from the results of tests of submerged inlets on a 1/4-scale model of a hypothetical turbine-propeller-driven fighter airplane.

1. The effect of a propeller is detrimental to the ram-pressure recovery of submerged inlets if the shank sections of the blades do not provide positive thrust.
2. The rate of increase of ram-pressure recovery with thrust coefficient was approximately the same at the entrance to the inlets as at the simulated entrance to the compressor.
3. The rate of increase in ram-pressure recovery with thrust coefficient was relatively independent of inlet-velocity ratio, but decreased with increasing propeller-blade angle and with angle of attack.
4. For the model investigated, the ram-recovery ratio was reduced approximately 0.06 by the propeller for conditions simulating flight at 500 miles per hour. For conditions simulating climb at 250 miles per hour the propeller increased the ram-pressure recovery.

Ames Aeronautical Laboratory,  
National Advisory Committee for Aeronautics,  
Moffett Field, Calif.



## APPENDIX

## Pertinent Dimensions of the Model

## Model

Wing area . . . . .	14.519 sq ft
Wing span . . . . .	8.50 ft
Tip chord . . . . .	1.146 ft
Root chord . . . . .	2.292 ft
Aspect ratio . . . . .	4.98
Taper ratio . . . . .	0.5
Wing incidence . . . . .	0°
Wing section . . . . .	NACA 63 <sub>1</sub> -110
Assumed wing loading . . . . .	36.45 lb per sq ft

## Propeller

## Number of blades

Front . . . . .	4
Rear . . . . .	4

Diameter . . . . . 3 ft

Blade section . . . . . NACA 16 series

## Activity factor

Front . . . . .	98.8
Rear . . . . .	98.0

## Spinner diameter at blade center line

Front blades . . . . .	20.2-percent propeller diameter
Rear blades . . . . .	26.0-percent propeller diameter



## Submerged Inlets

Ramp angle . . . . .	7°
Width-to-depth ratio of inlets . . . . .	4
Total inlet area (both ducts) measured 1½ inches behind lip leading edge . . . . .	0.0718 sq ft
Depth of ramp at the lip leading edge . . . . .	1.720 in.
Distance of duct-lip leading edge ahead of wing leading edge . . . . .	19.3-percent root chord
Distance of duct center line below thrust axis . . . . .	1.05 in.
Distance of duct-lip leading edge behind plane of rear propeller blades . . . . .	20.66 in.
Diffuser area ratio ( $A_2/A_1$ ) . . . . .	1.336
Diffuser efficiency (determined from bench tests, reference 1) . . . . .	89 to 90 percent

## REFERENCES

1. Delany, Noel K.: An Investigation of Submerged Air Inlets on a 1/4-Scale Model of a Typical Fighter-Type Airplane. NACA RM A8A20, 1948.
2. Hall, Charles F., and Barclay, F. Dorn: An Experimental Investigation of NACA Submerged Inlets at High Subsonic Speeds. I - Inlets Forward of the Wing Leading Edge. NACA RM A8B16, 1948.
3. Delano, James B., and Carmel, Melvin M.: Effect of Shank Design on Propeller Performance at High Speeds. NACA ARR L6D23, 1946.
4. Hall, Charles F., and Frank, Joseph L.: Ram-Recovery Characteristics of NACA Submerged Inlets at High Subsonic Speeds. NACA RM A8I29, 1948.



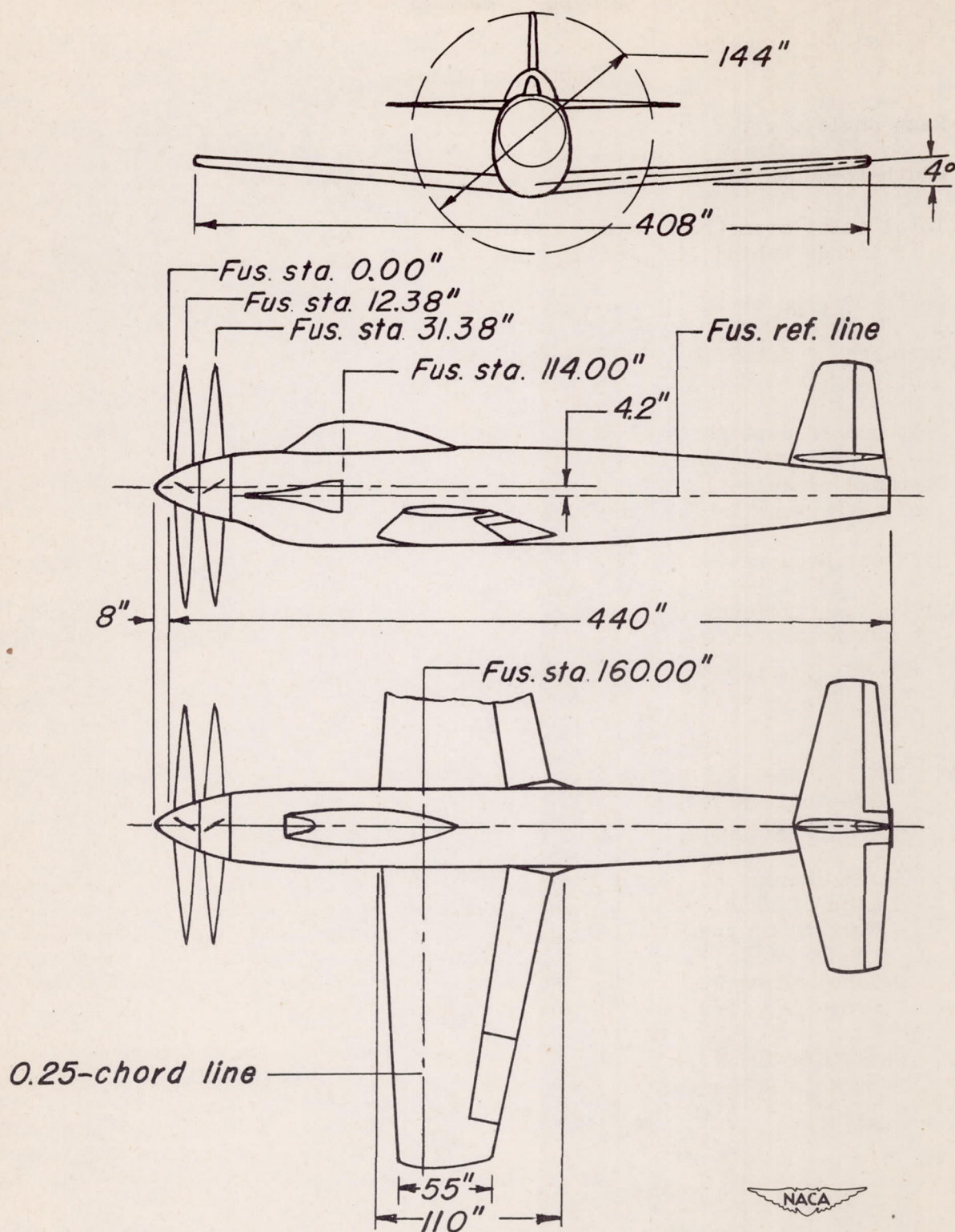


Figure 1.—Three-view drawing of the hypothetical airplane simulated by the  $\frac{1}{4}$ -scale model.







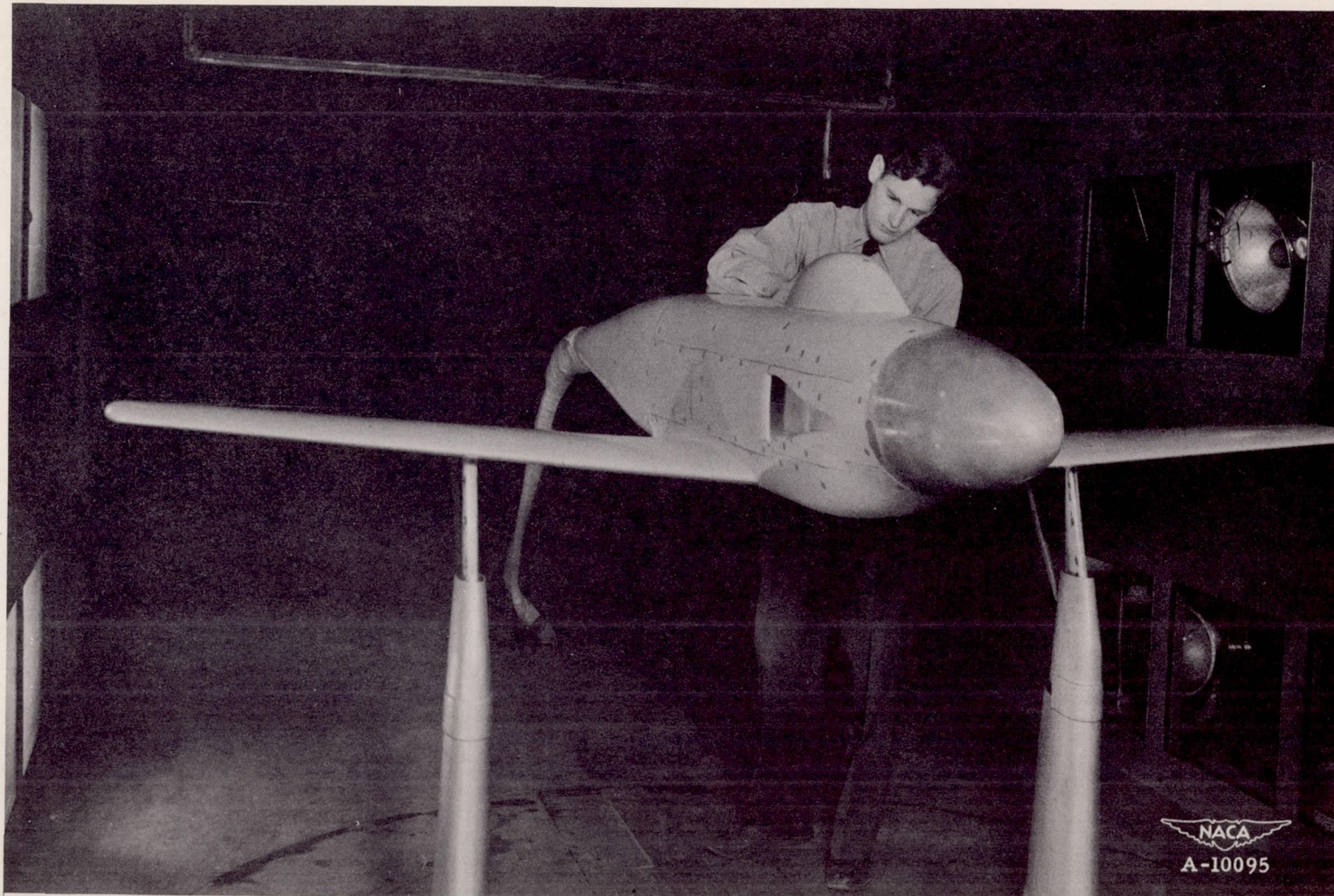
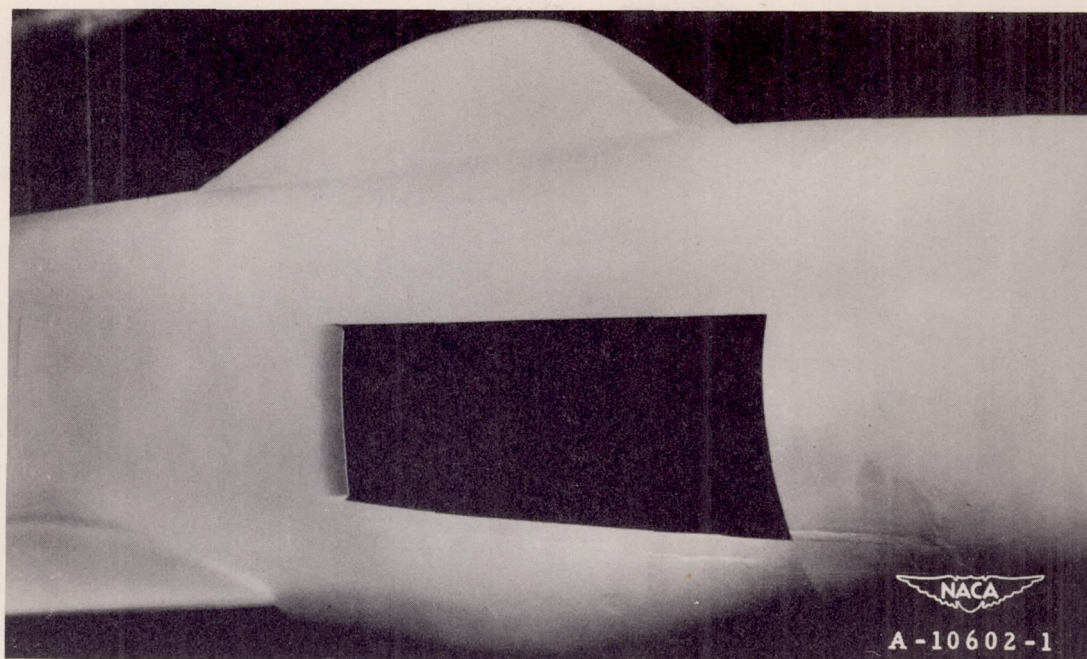


Figure 2.- The model installed in the Ames 7- by 10-foot wind tunnel No. 2.

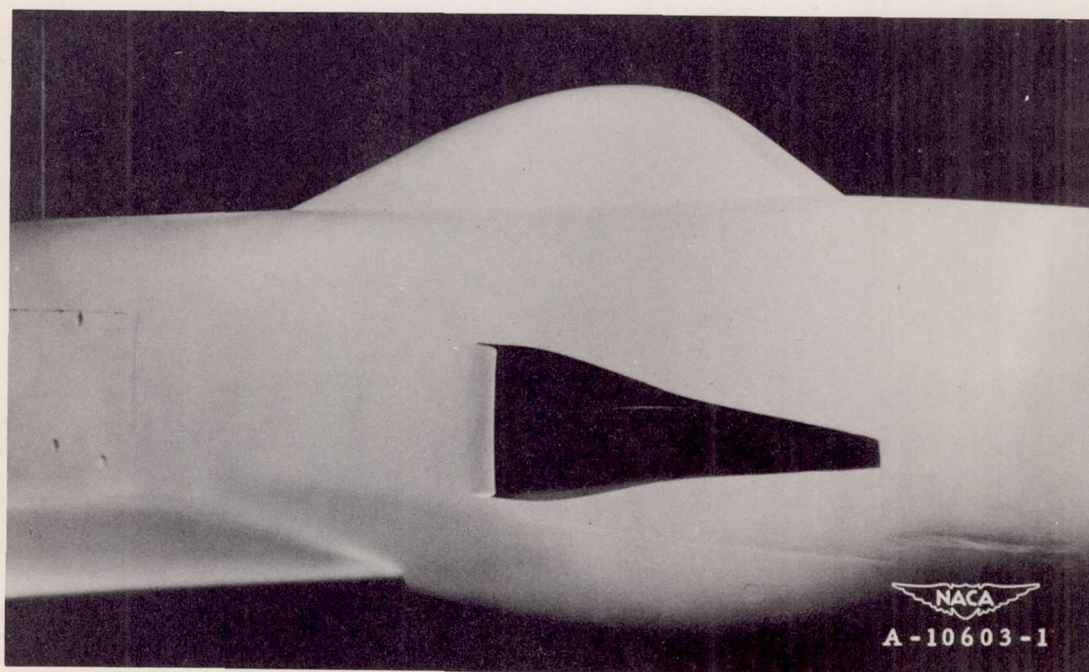








(a) Inlet with parallel ramp walls .



(b) Inlet with diverging ramp walls.

Figure 3.- Photographs of the submerged inlets tested.







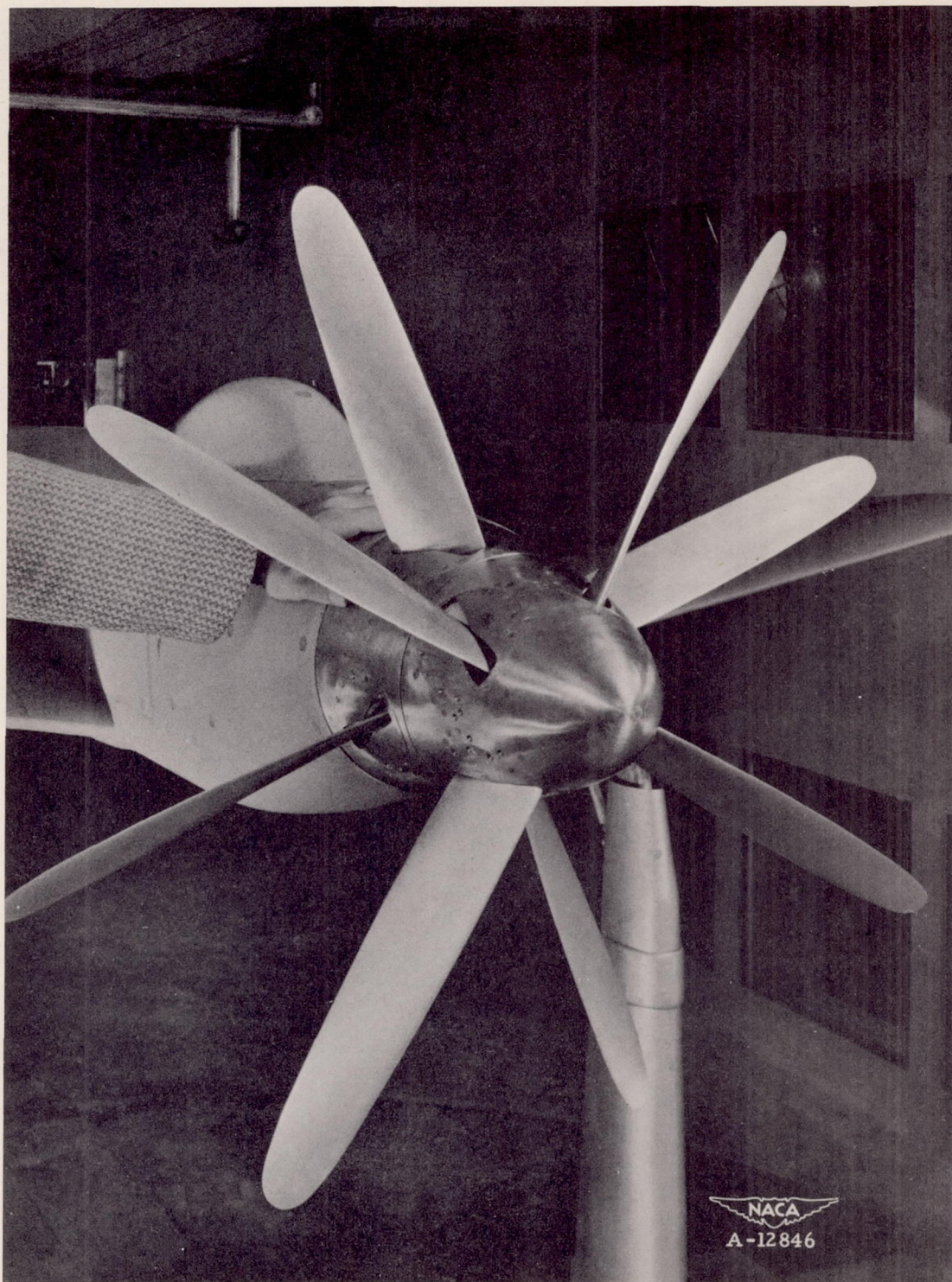


Figure 4.- Photograph of eight-blade dual-rotation model propeller.







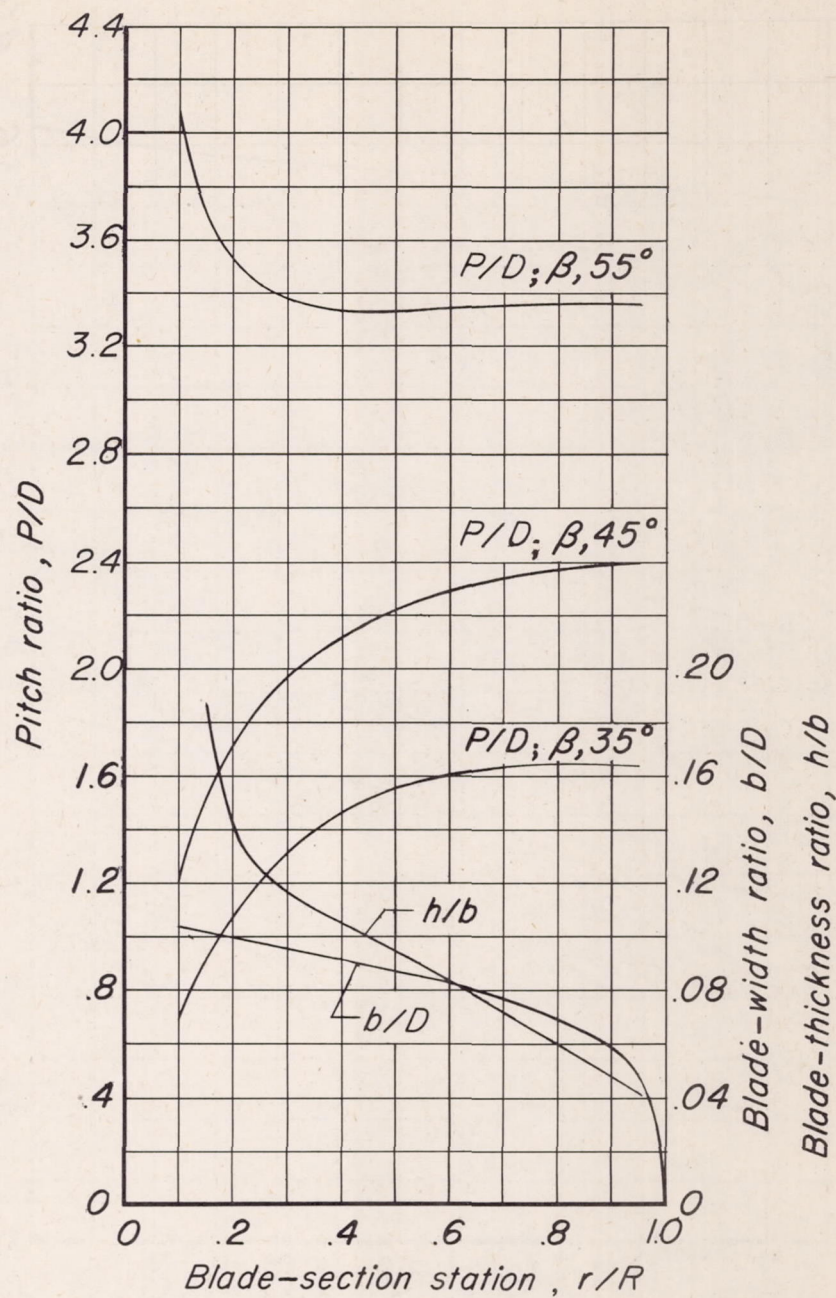


Figure 5. - Blade-form curves for the NACA 3-(3.9)(07)-0345-A propeller.



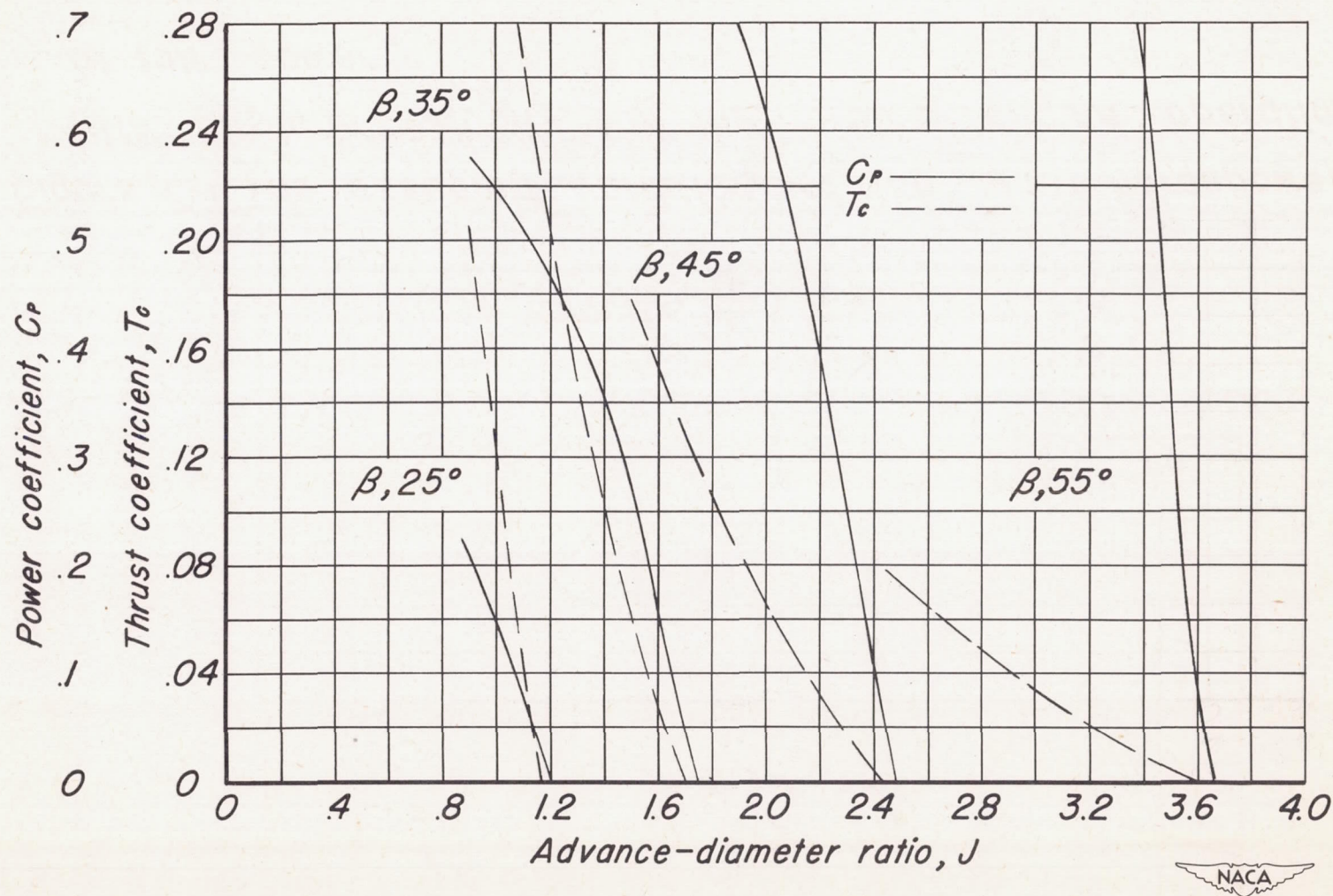


Figure 6.—Aerodynamic characteristics of the NACA 3-(3.9)(07)-0345-A model propeller tested.



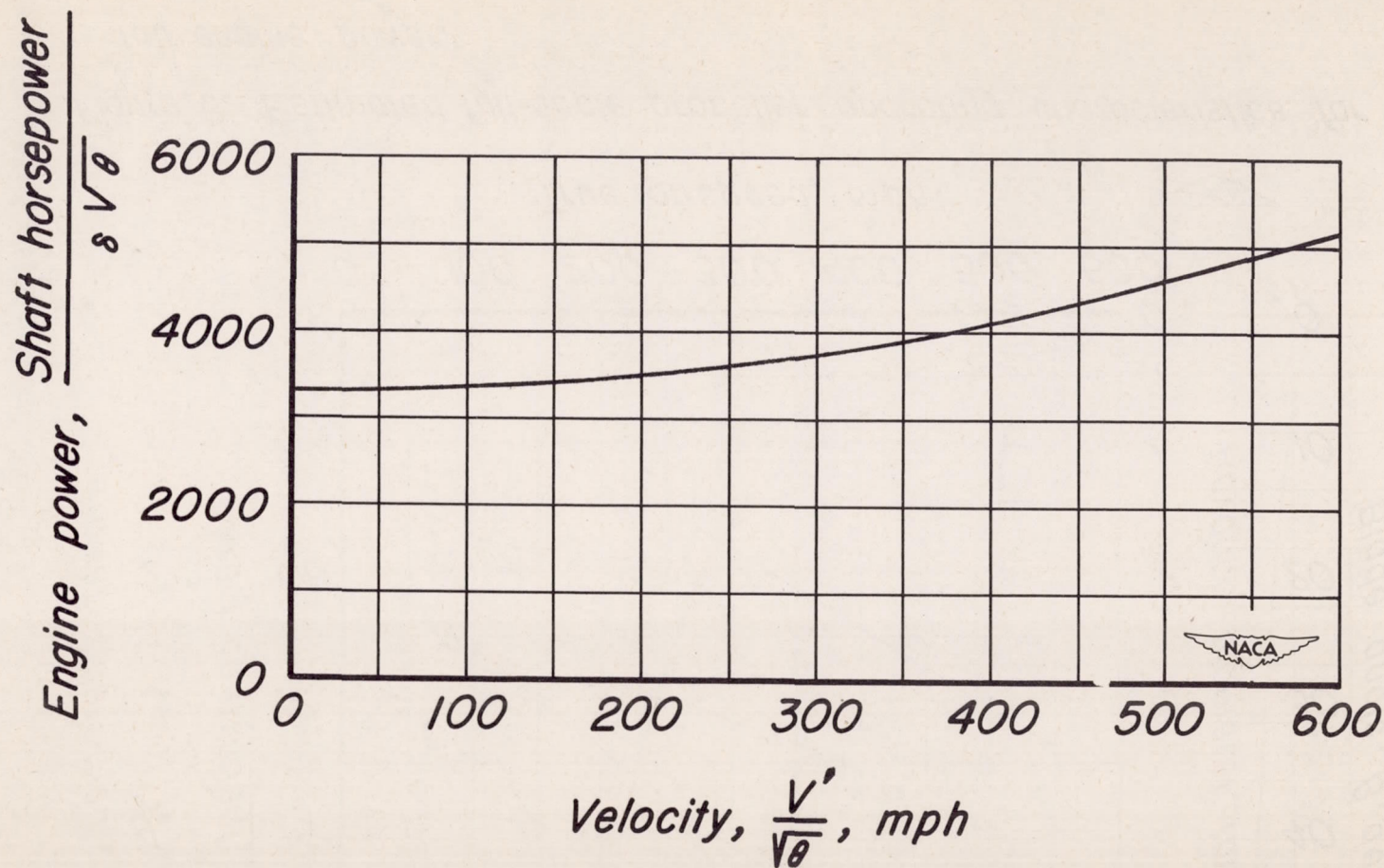


Figure 7.- The assumed variation of the shaft horsepower with airplane velocity for the turbine engine operating at full power.



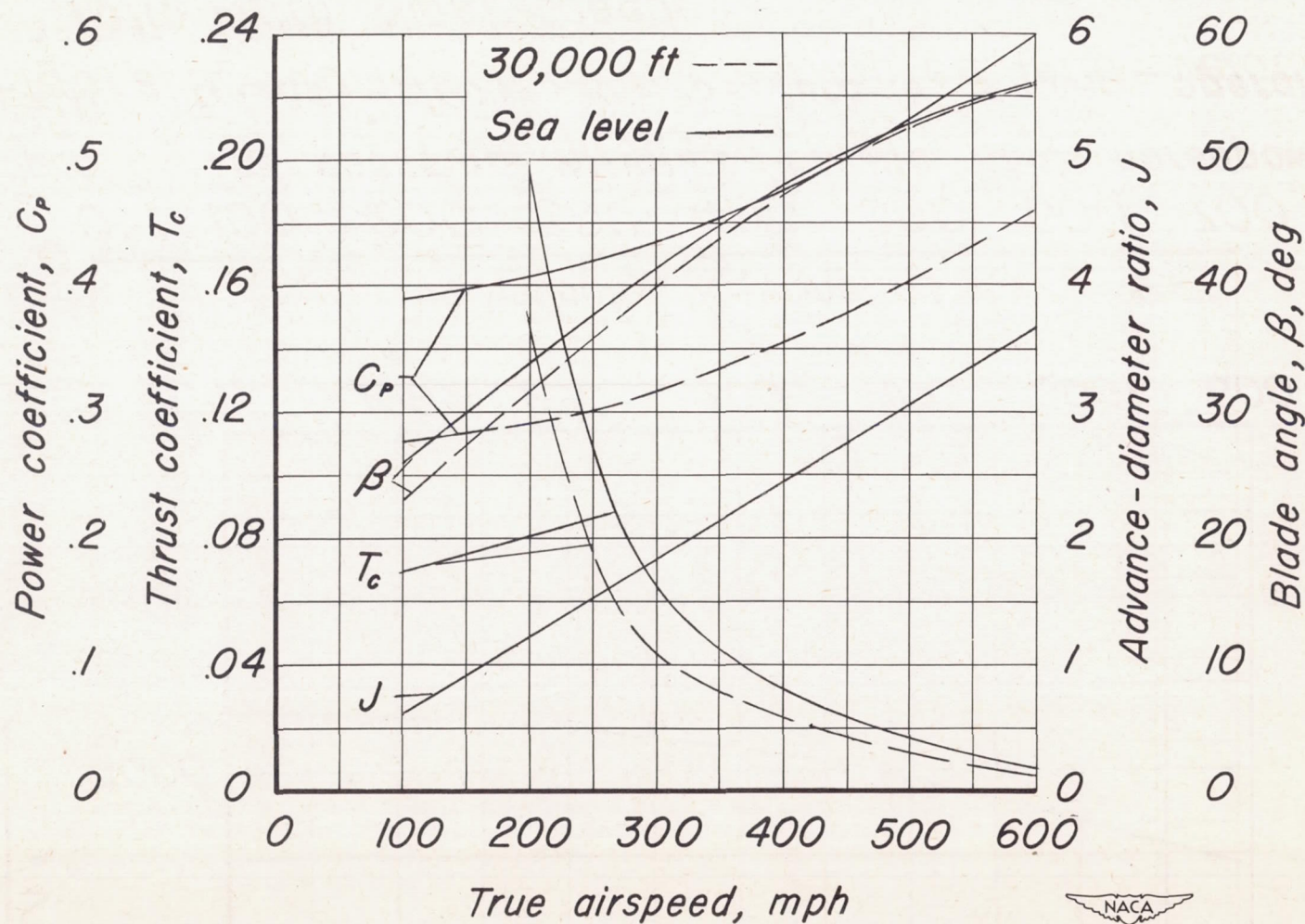


Figure 8.- Estimated full-scale propeller operating characteristics for full engine power.



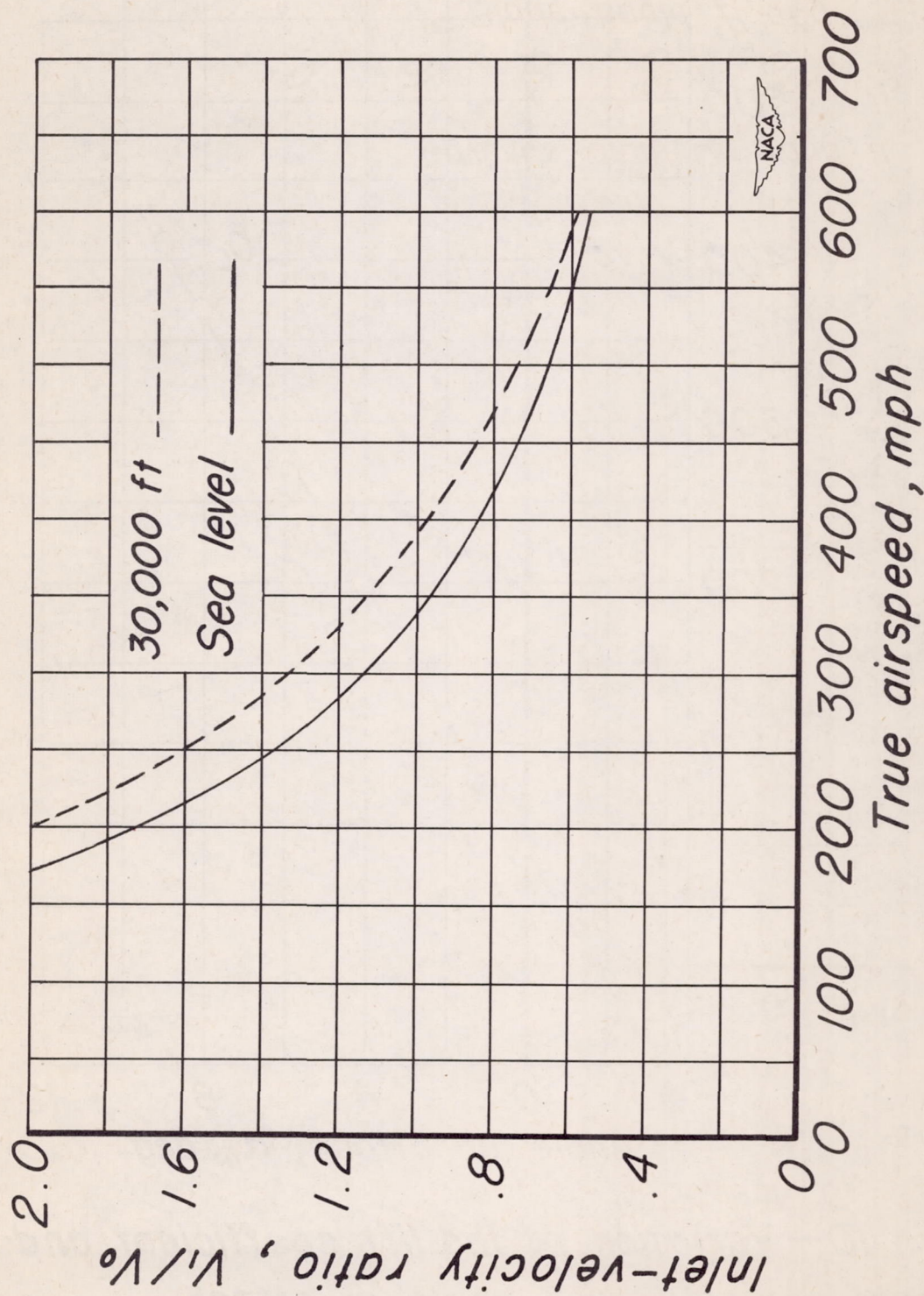
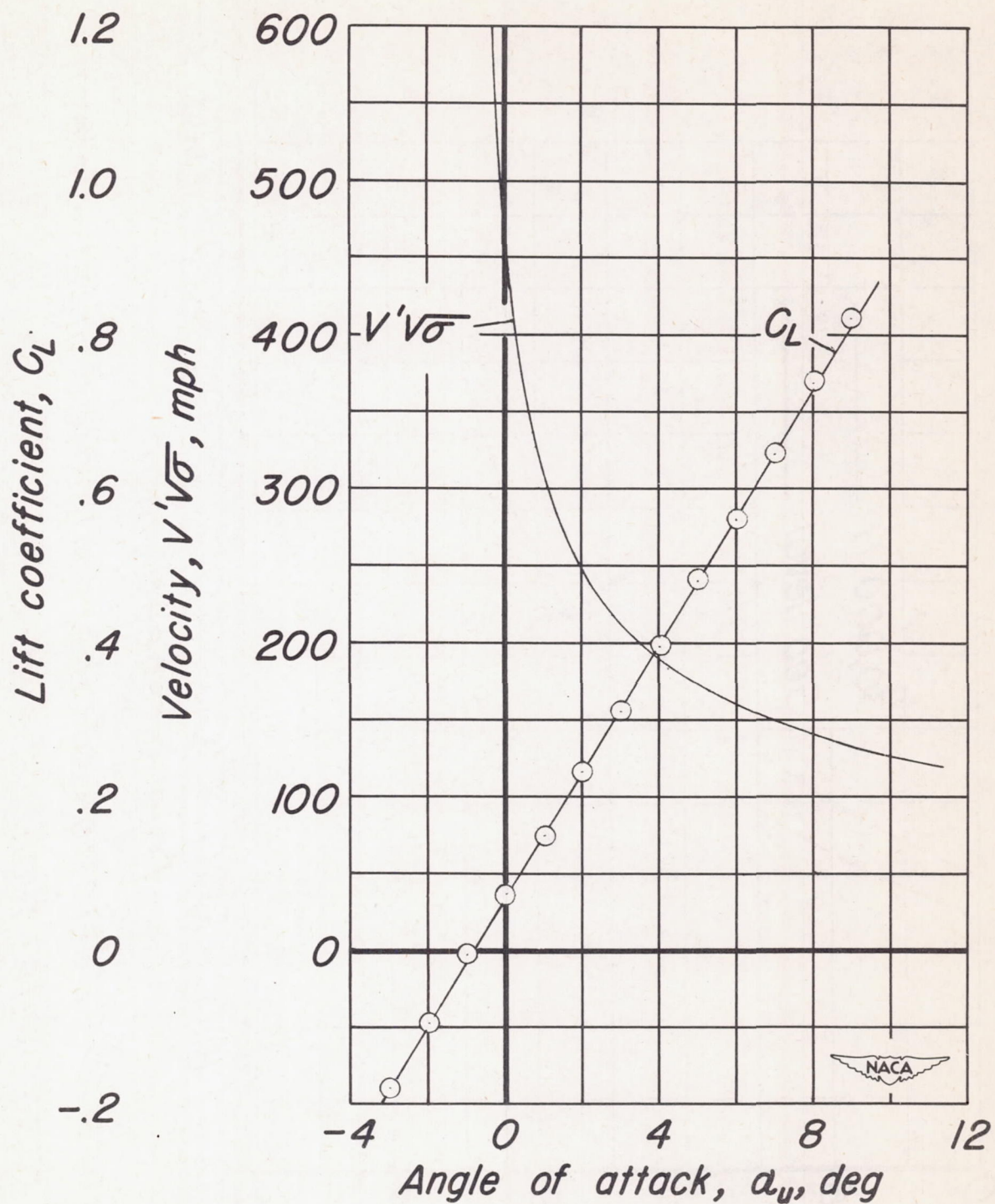


Figure 9.— Variation of the estimated inlet-velocity ratio with flight speed.







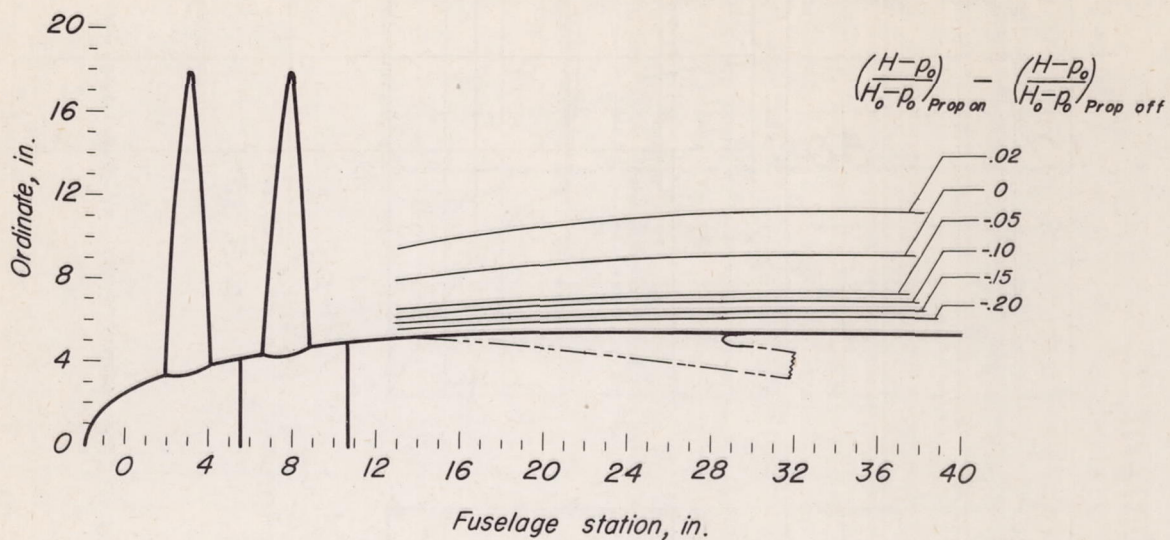
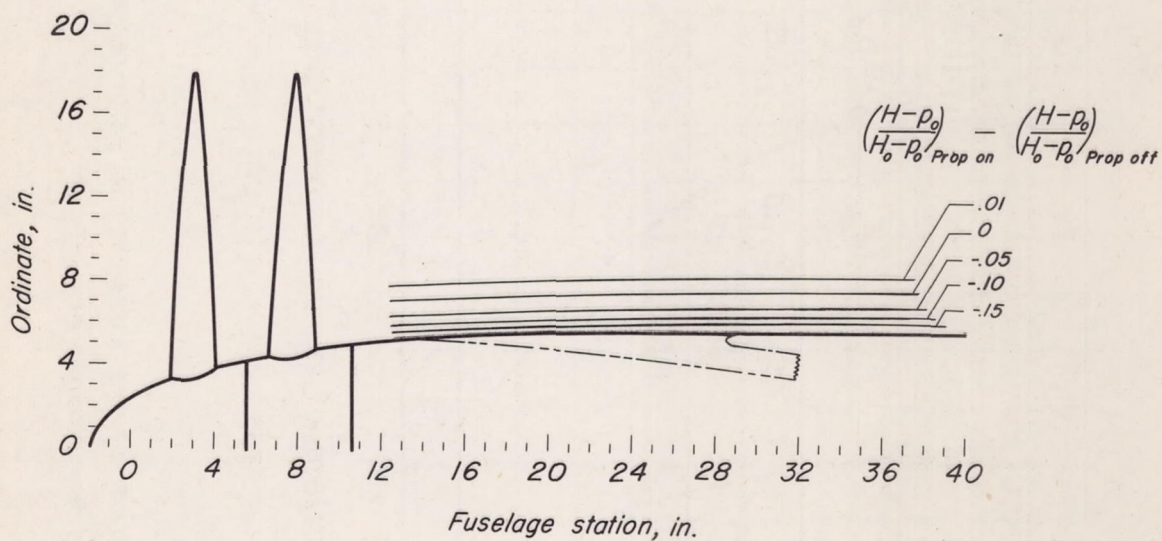
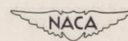
(a)  $\beta, 35^\circ$ .(b)  $\beta, 55^\circ$ .

Figure 11.— Variation of the increment in ram-recovery ratio in the slipstream due to the propeller.  $T_c, 0$ ;  $a_u, 0^\circ$ .



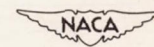
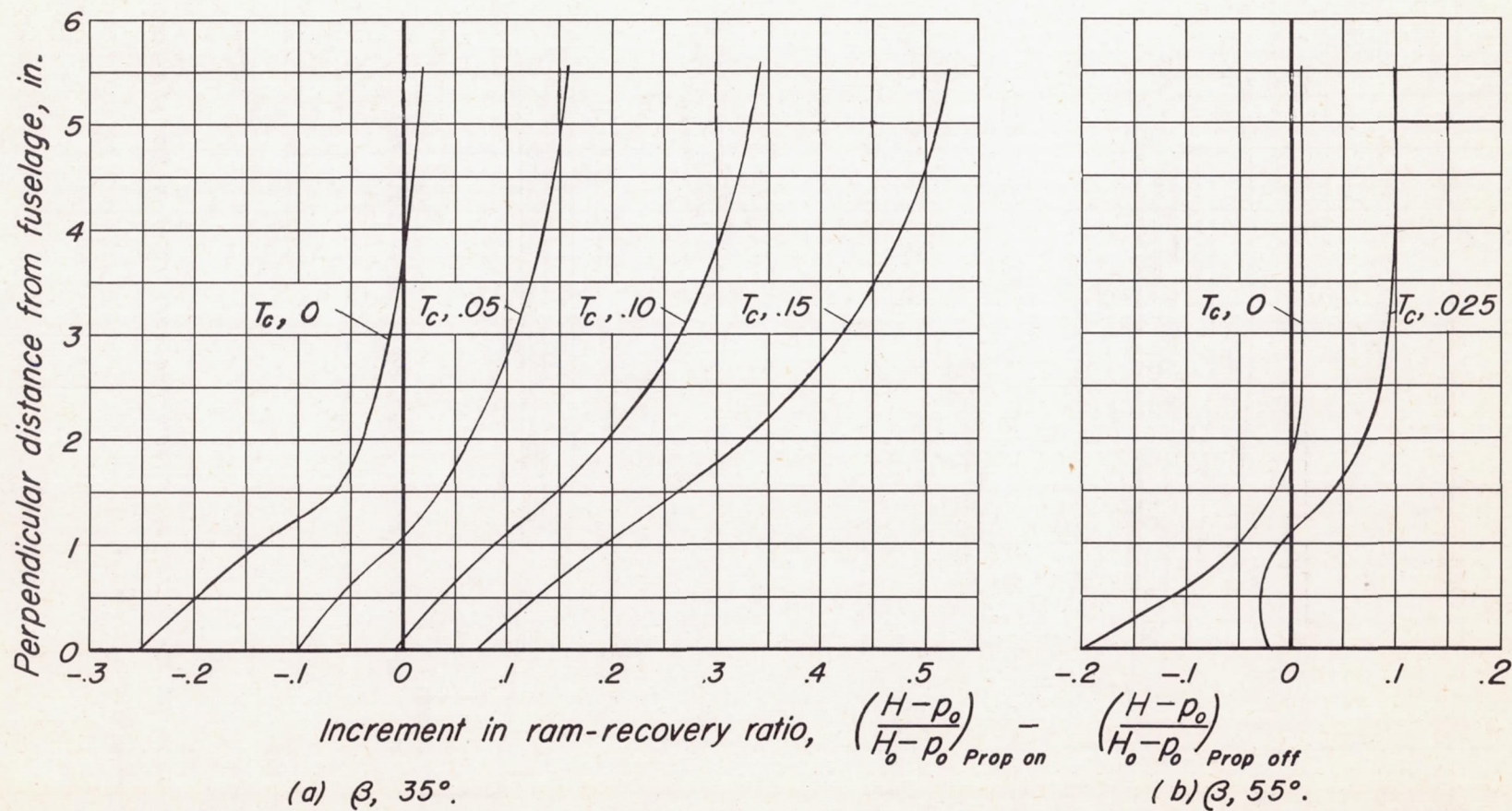


Figure 12.—Variation of the increment in ram-recovery ratio in the slipstream at the duct-inlet station due to the propeller.  $\alpha_u, 0^\circ$ .



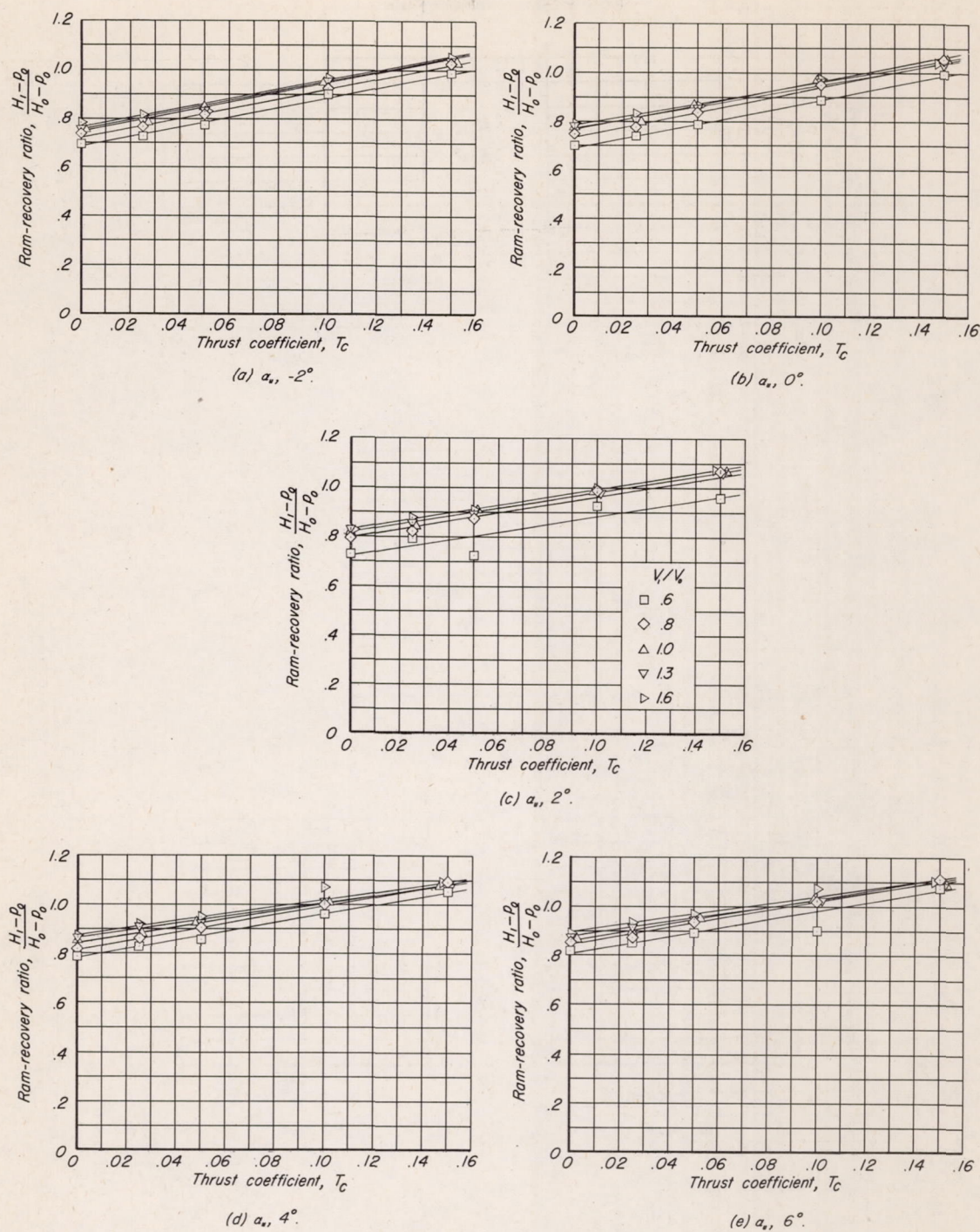


Figure 13.— Variation with thrust coefficient of the ram-recovery ratio at the inlet for the inlets with parallel ramp walls.  $\beta, 35^\circ$ .



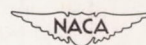
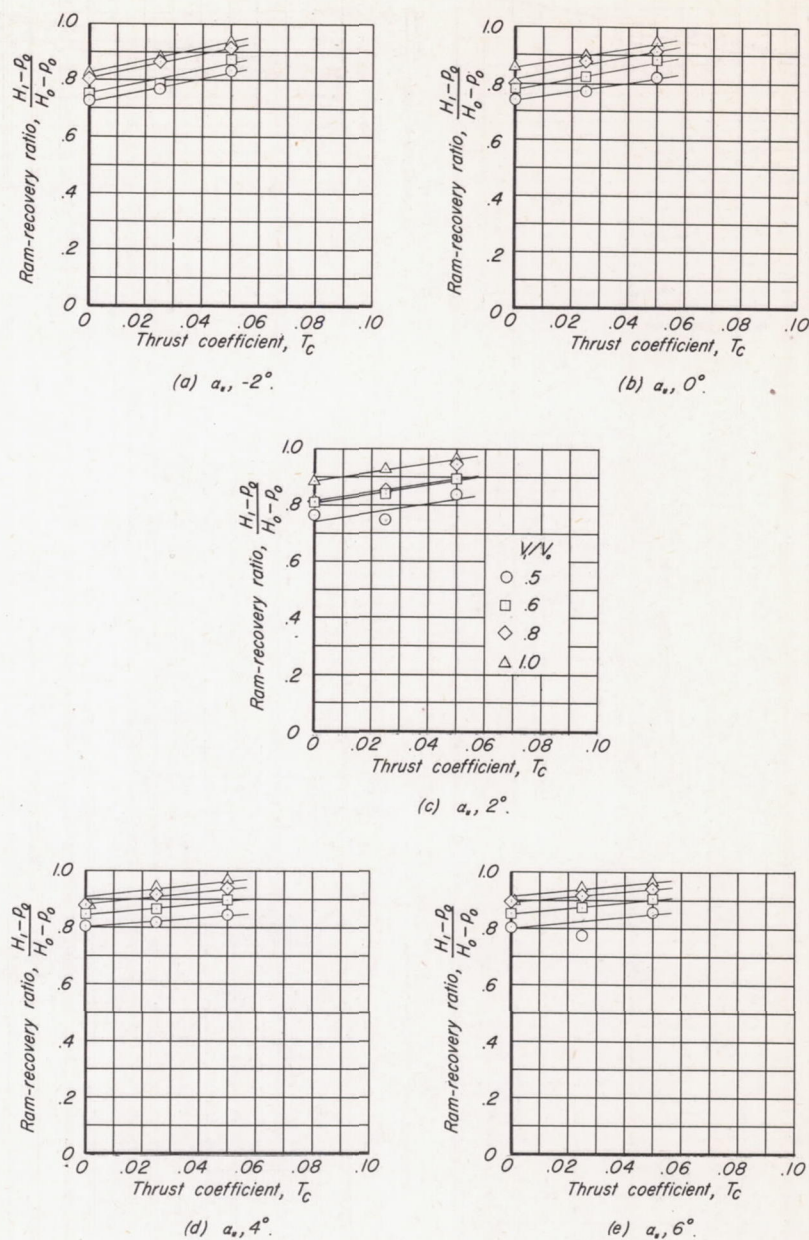


Figure 14.—Variation with thrust coefficient of the ram-recovery ratio at the inlet for the inlets with parallel ramp walls.  $\beta, 55^\circ$ .



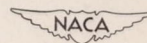
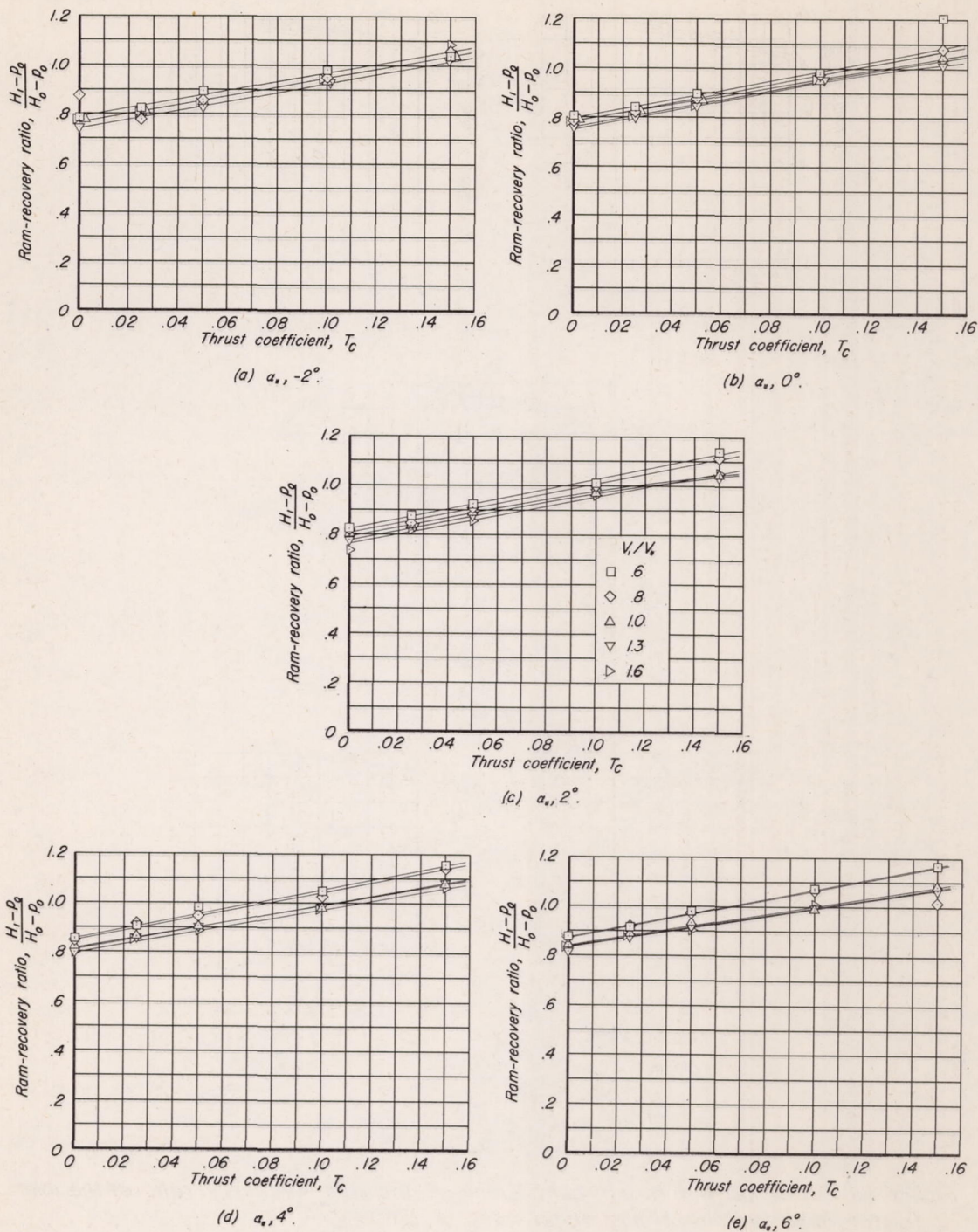


Figure 15.— Variation with thrust coefficient of the ram-recovery ratio at the inlet for the inlets with diverging ramp walls.  $\beta, 35^\circ$ .



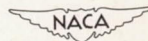
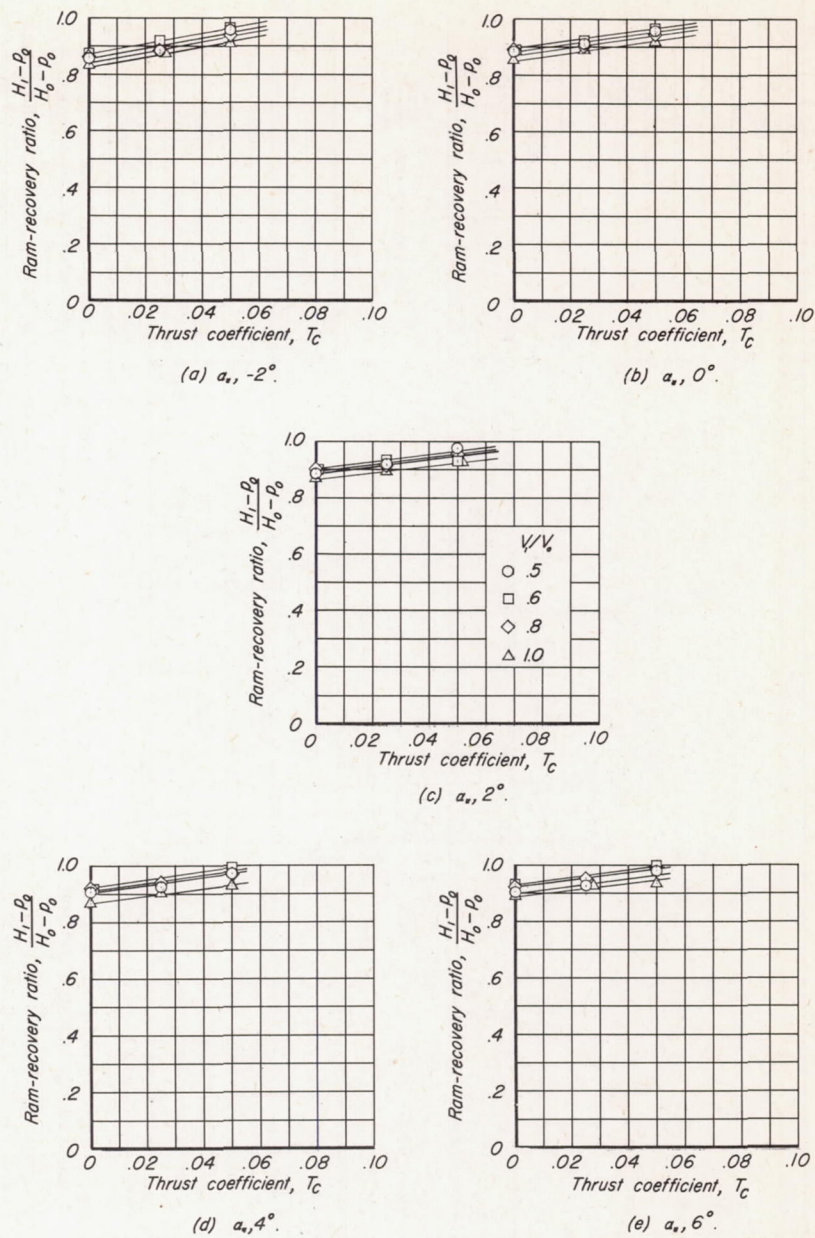


Figure 16.— Variation with thrust coefficient of the ram—recovery ratio at the inlet for the inlets with diverging ramp walls.  $\beta, 55^\circ$ .



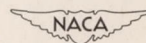
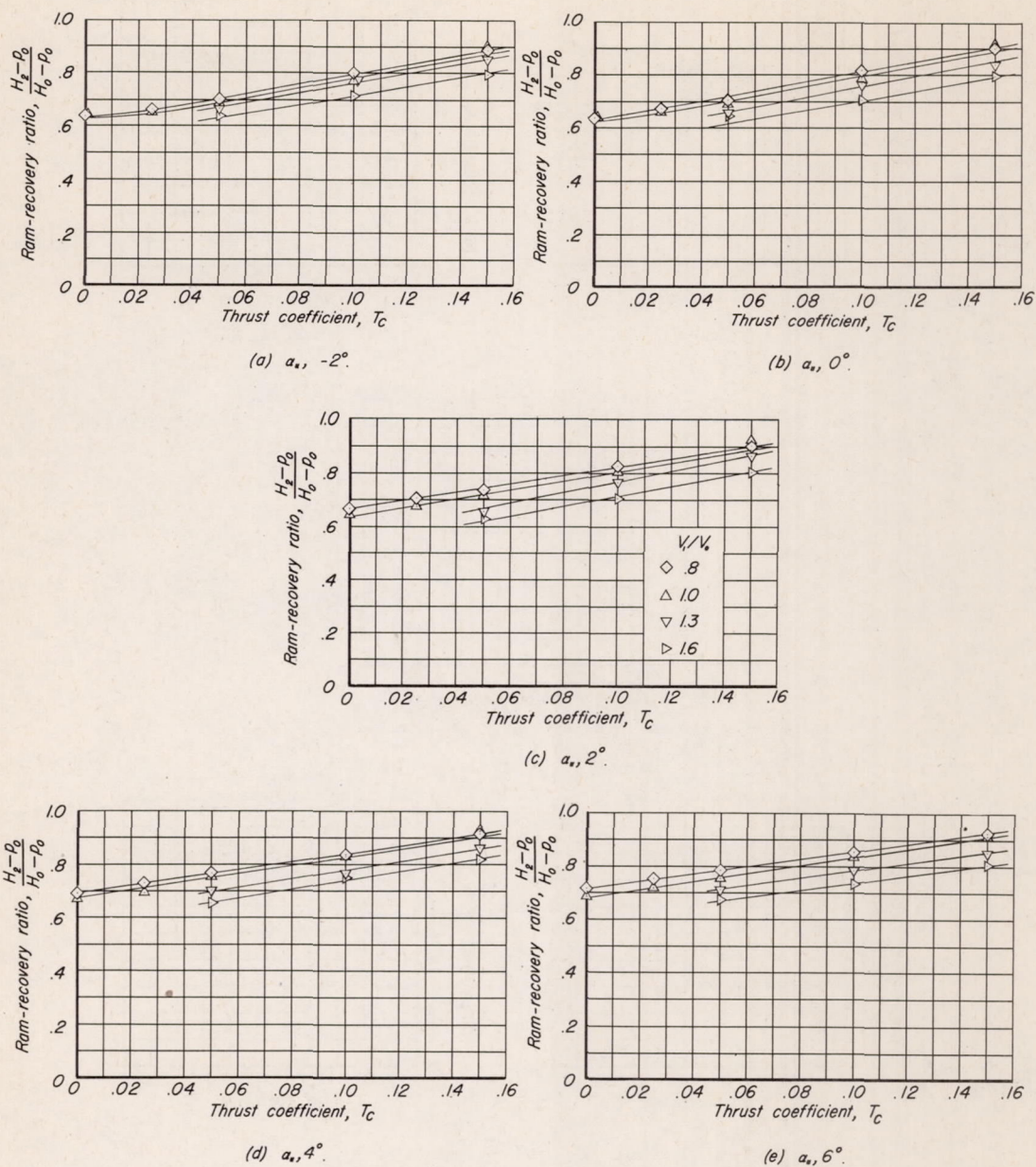


Figure 17— Variation with thrust coefficient of the ram-recovery ratio at the simulated compressor entrance for the inlets with parallel ramp walls.  $\beta, 35^\circ$ .



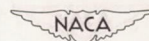
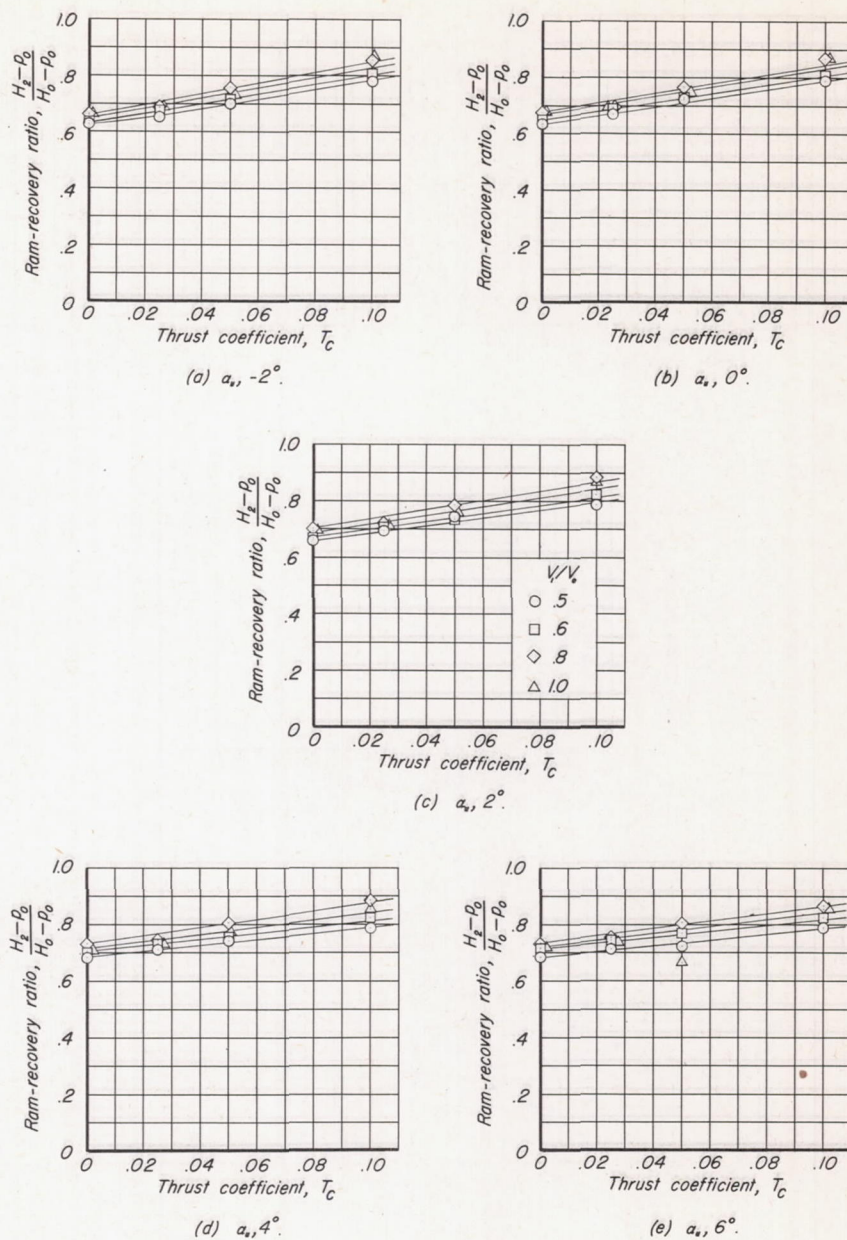


Figure 18.—Variation with thrust coefficient of the ram-recovery ratio at the simulated compressor entrance for the inlets with parallel ramp walls.  $\beta, 45^\circ$ .



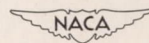
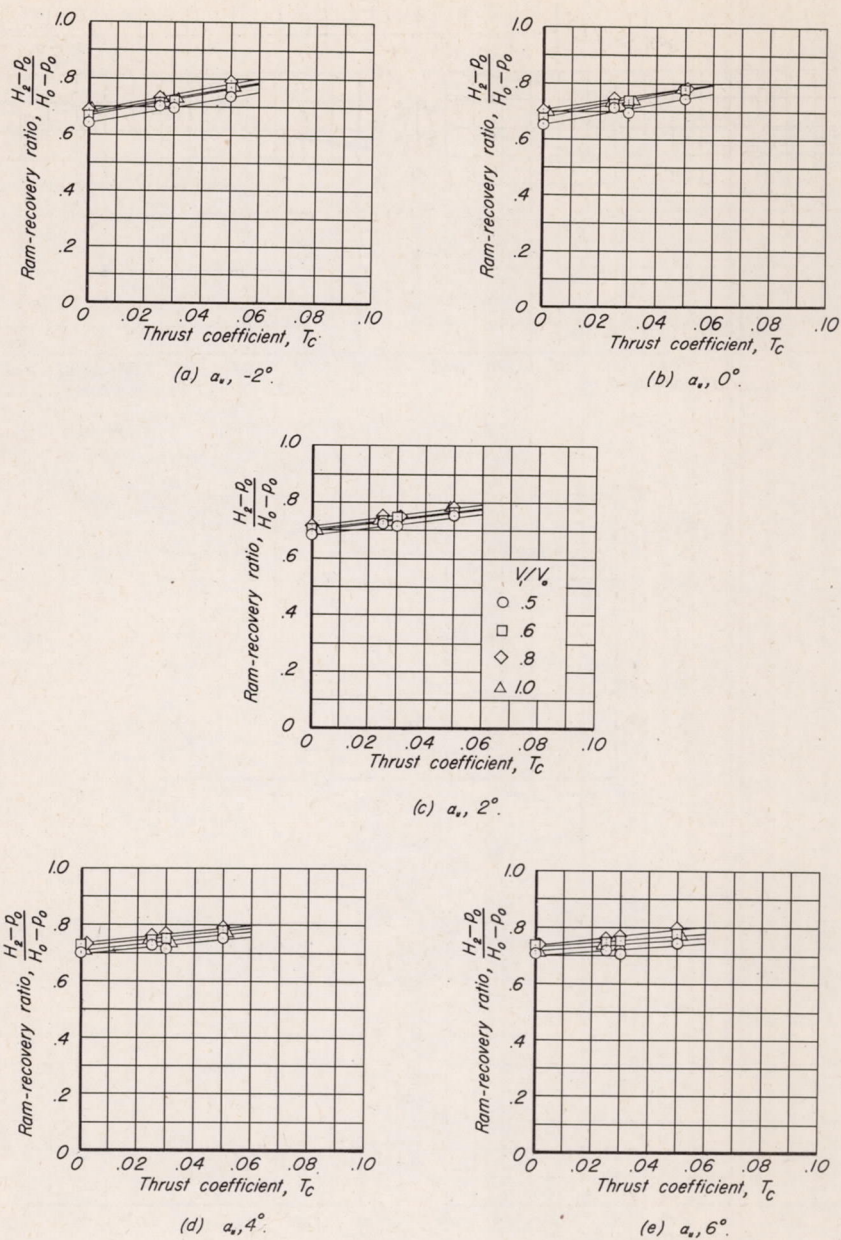


Figure 19.—Variation with thrust coefficient of the ram-recovery ratio at the simulated compressor entrance for the inlets with parallel ramp walls.  $\beta, 55^\circ$ .



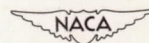
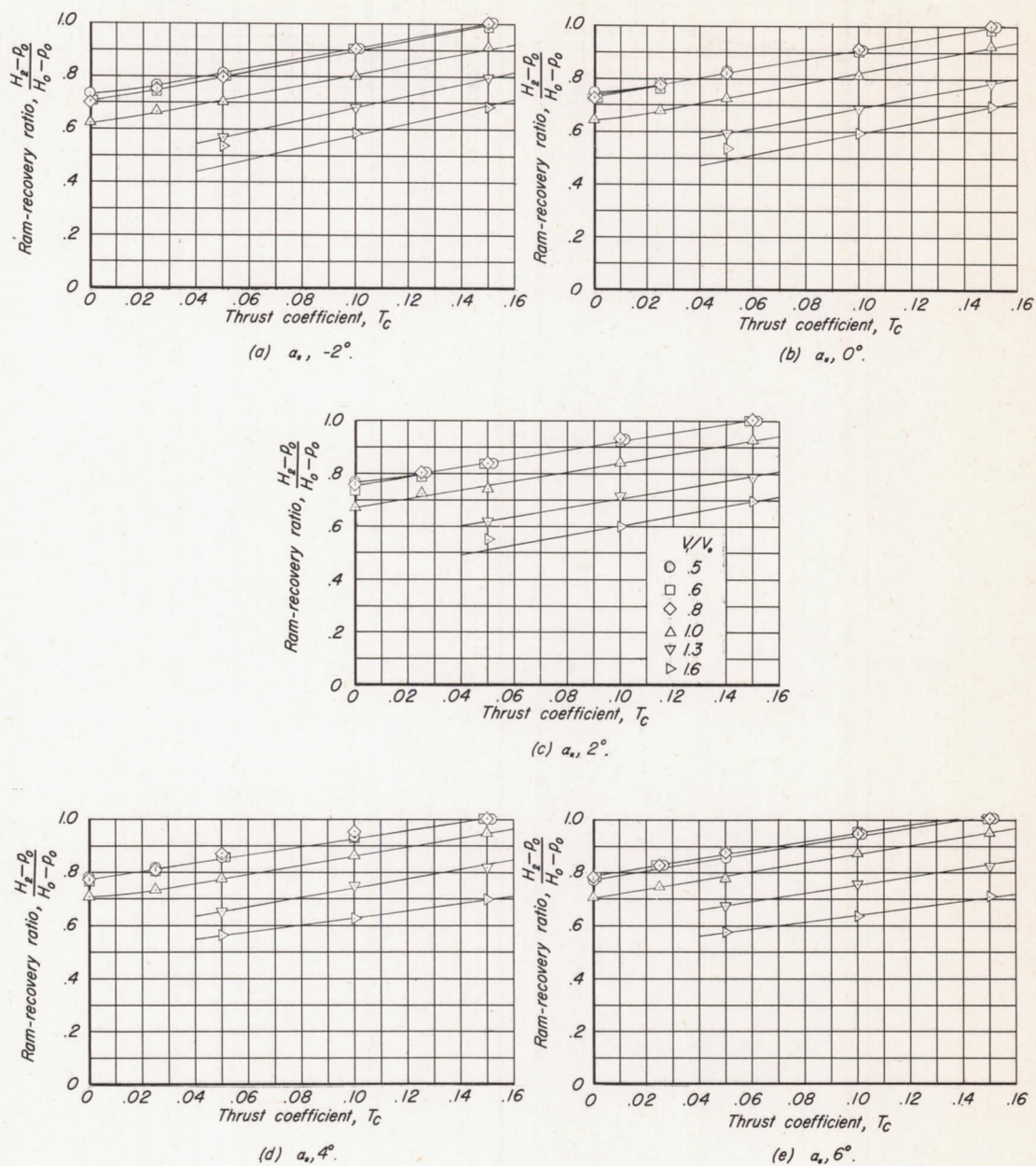


Figure 20.—Variation with thrust coefficient of the ram-recovery ratio at the simulated compressor entrance for the inlets with diverging ramp walls.  $\beta, 35^\circ$ .



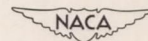
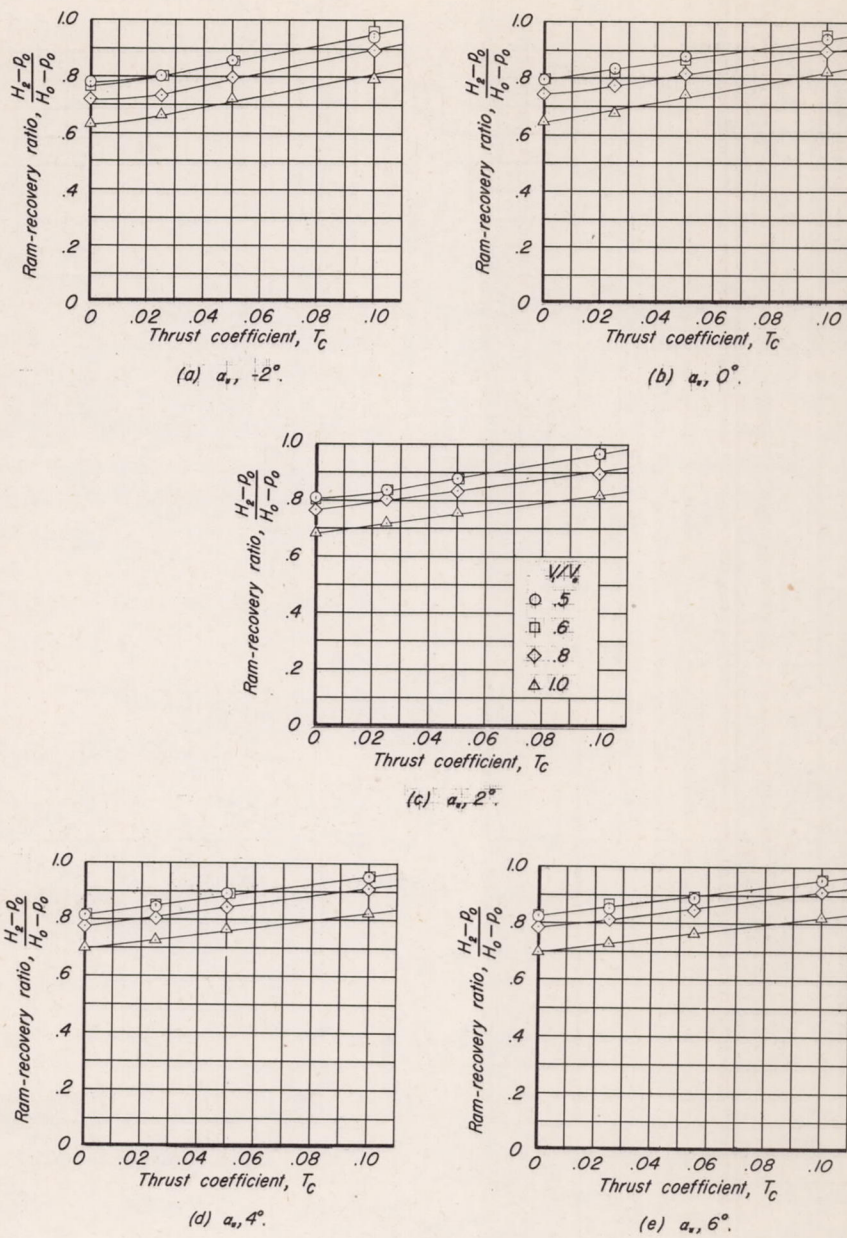


Figure 21.—Variation with thrust coefficient of the ram-recovery ratio at the simulated compressor entrance for the inlets with diverging ramp walls.  $\beta, 45^\circ$ .



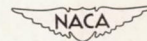
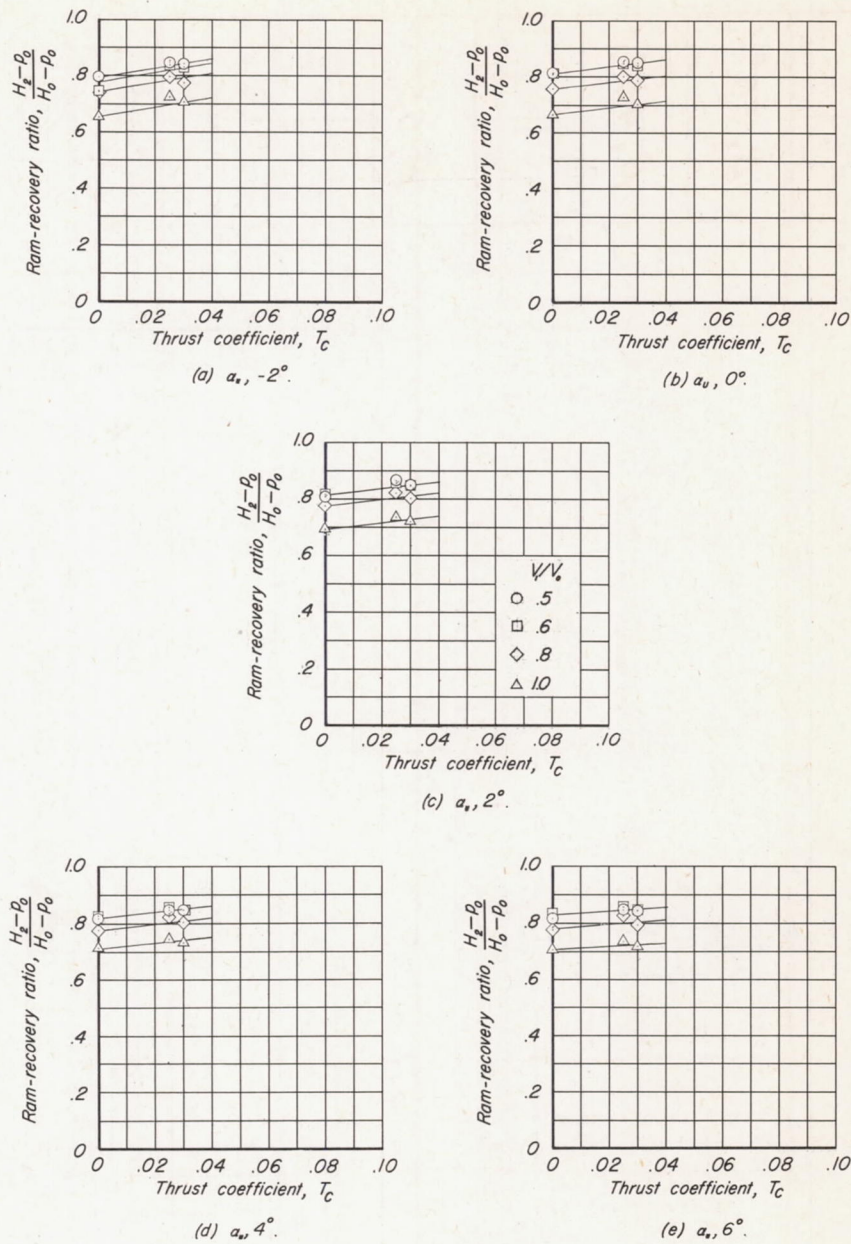


Figure 22—Variation with thrust coefficient of the ram-recovery ratio at the simulated compressor entrance for the inlets with diverging ramp walls.  $\beta, 55^\circ$ .



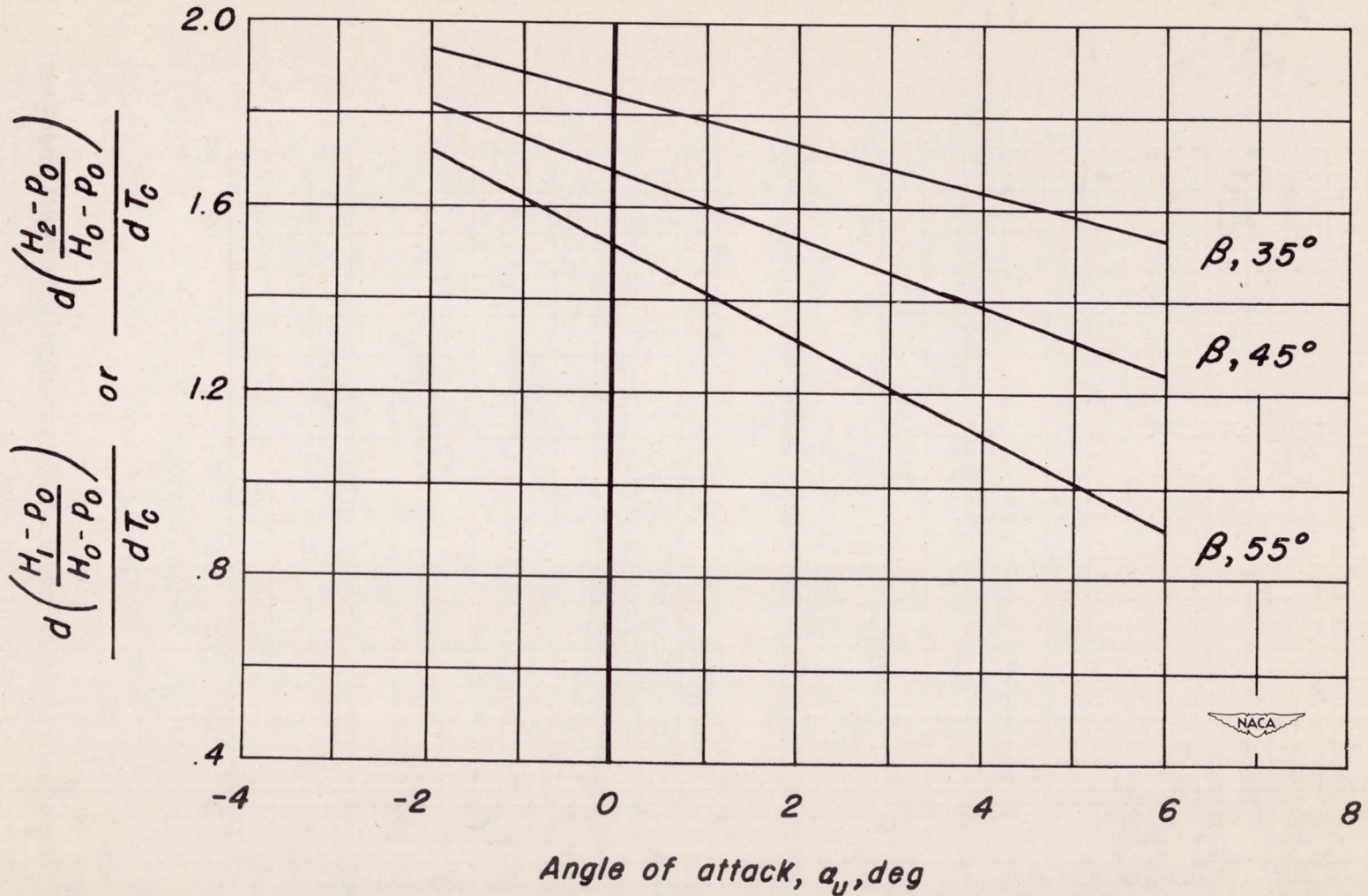
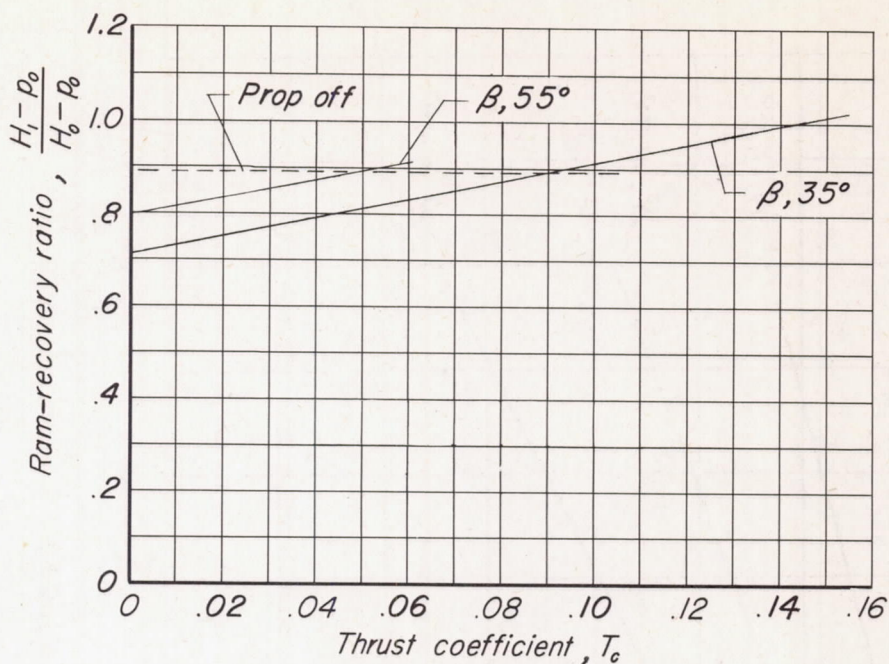
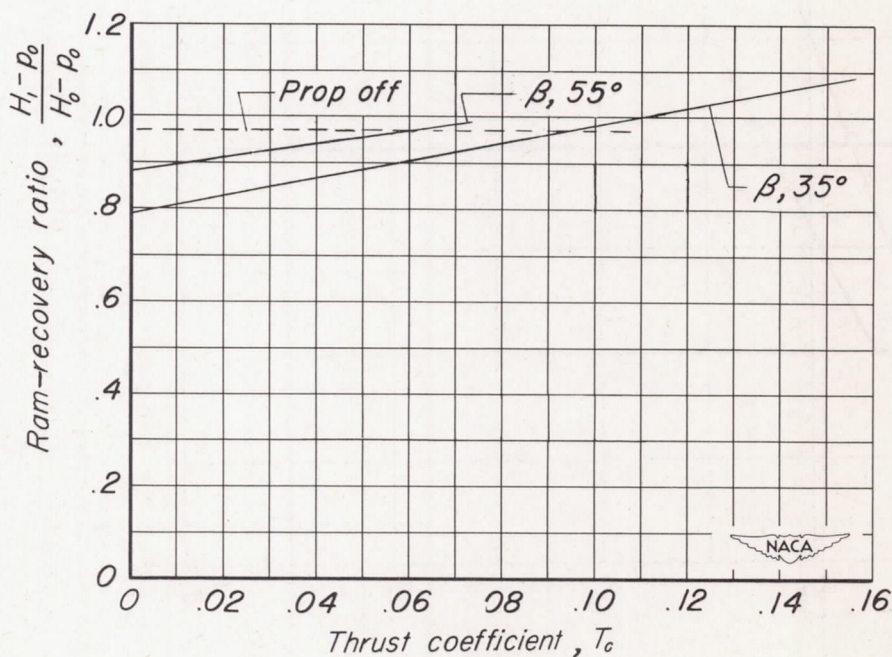


Figure 23.—The effect of propeller-blade angle and angle of attack on the average rate of change of ram-recovery ratio with thrust coefficient.





(a) Parallel walls.



(b) Divergent walls.

Figure 24.—The effect of blade angle on the variation with thrust coefficient of the ram-recovery ratio at the inlet.  $V_1/V_0$ , 0.7;  $\alpha_0$ ,  $0^\circ$ .



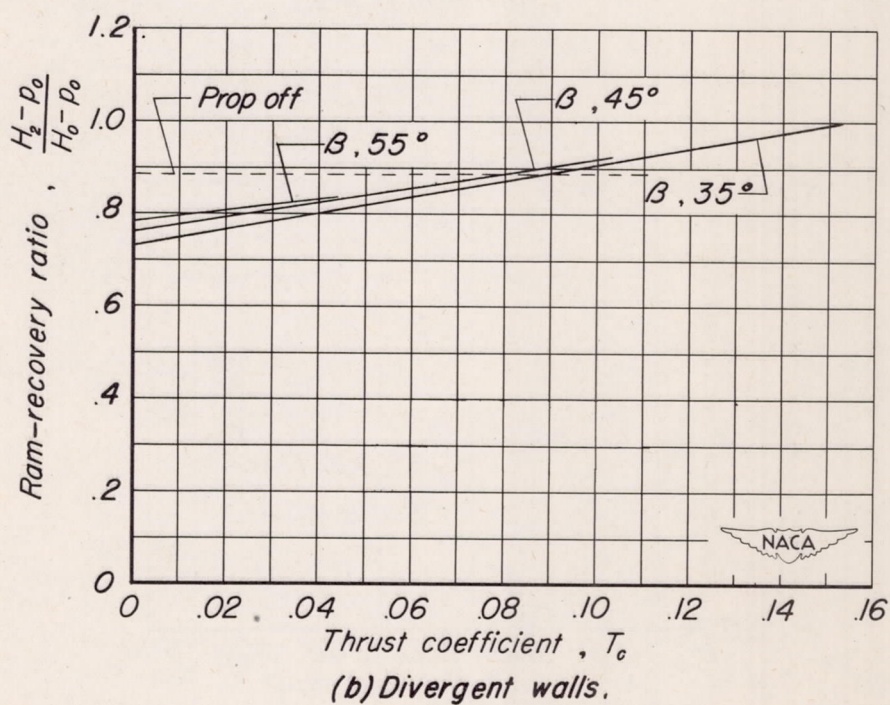
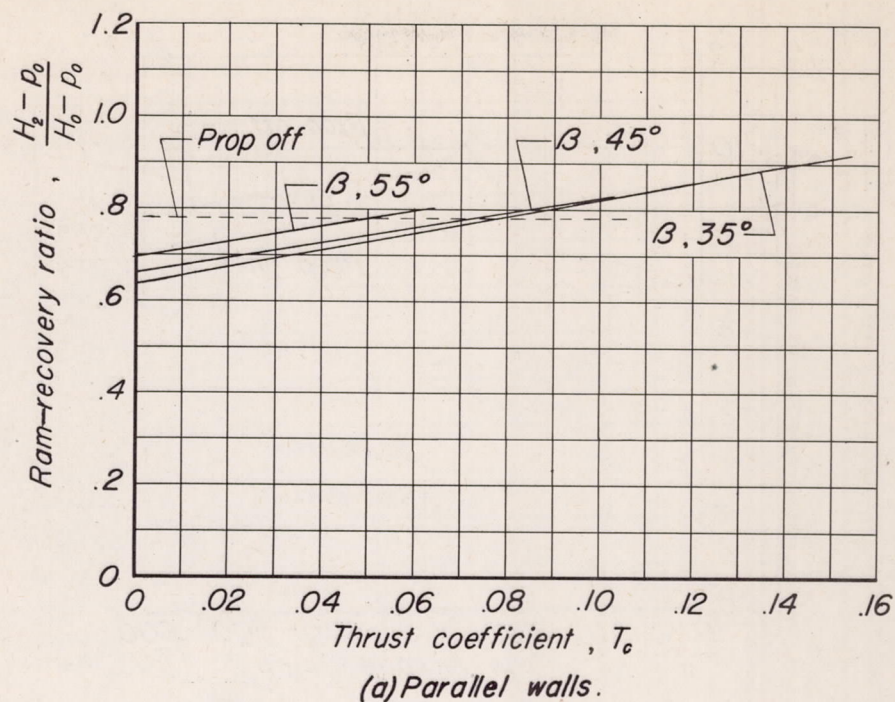
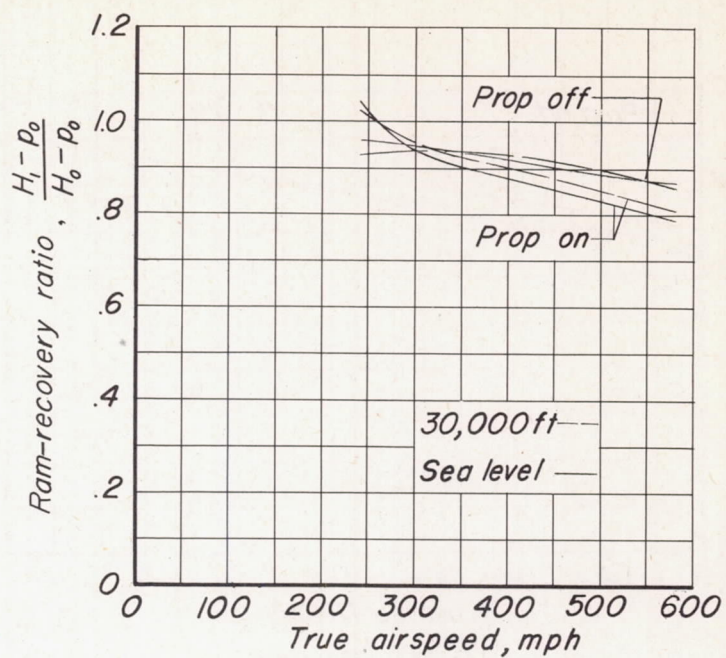
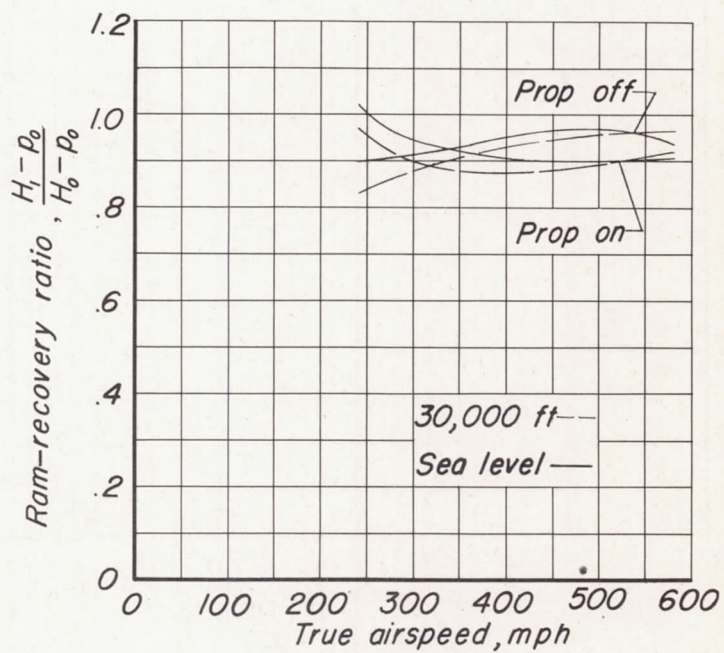


Figure 25.—The effect of blade angle on the variation with thrust coefficient of the ram-recovery ratio at the simulated compressor entrance.  
 $V_1/V_0$ , 0.7;  $\alpha_1$ ,  $0^\circ$ .





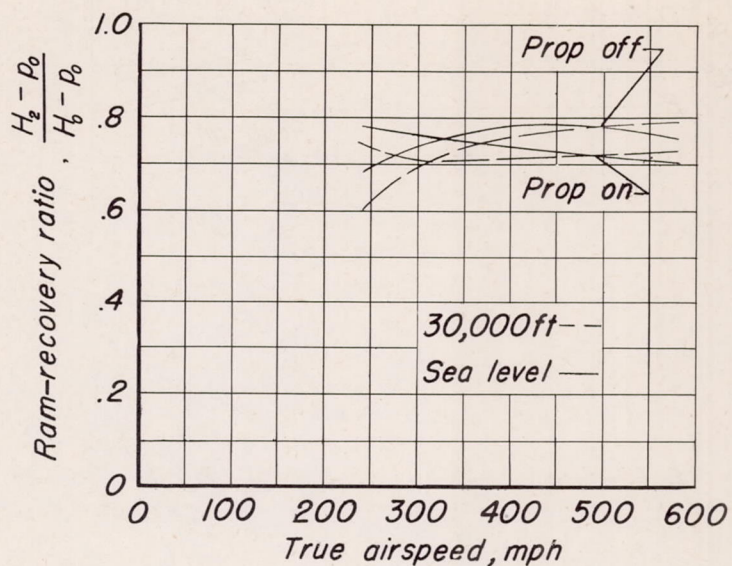
(a) Parallel walls.



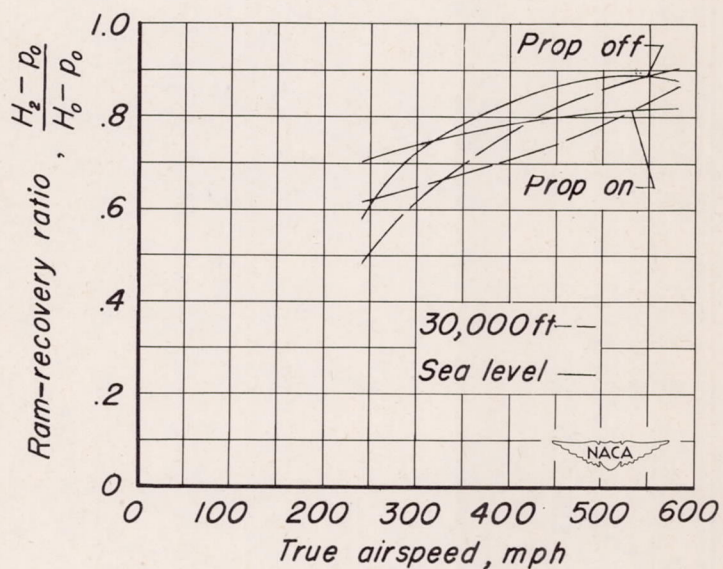
(b) Divergent walls.

Figure 26.—The effect of the propeller on the ram-recovery ratio at the inlet for simulated airplane flight conditions.





(a) Parallel walls.



(b) Divergent walls.

Figure 27.—The effect of the propeller on the ram-recovery ratio at the compressor entrance for simulated flight conditions.